

# Removal of spurious solutions encountered in Helmholtz scattering resonance computations in $\mathbb{R}^d$

Juan C. Araujo C.<sup>1</sup>, Christian Engström<sup>2</sup>

---

## Abstract

In this paper we consider a sorting scheme for the removal of spurious scattering resonant pairs in two-dimensional electromagnetic problems and in three-dimensional acoustic problems. The novel sorting scheme is based on a Lippmann–Schwinger type of volume integral equation and can therefore be applied to graded material properties as well as piece-wise constant material properties. For TM/TE polarized electromagnetic waves and for acoustic waves, we compute first approximations of scattering resonances with finite elements. Then, we apply the novel sorting scheme to the computed eigenpairs and use it to remove spurious solutions in electromagnetic and acoustic scattering resonances computations at low computational cost. Several test cases with Drude-Lorentz dielectric resonators as well as with graded material properties are considered.

### Keywords:

Plasmon resonance, acoustic scattering resonances, Resonance modes, Nonlinear eigenvalue problems, Helmholtz problem, Pseudospectrum, PML, DtN, leaky modes, resonant states, quasi-normal modes

---

## 1. Introduction

The most common approach to approximate scattering resonances is to truncate the domain with a perfectly matched layer (PML) and discretize the differential equations with a finite element method. This result in approximations of the true resonances but in practice also a large number of solutions that are unrelated to the true resonances. Those *spurious eigenvalues* are a major problem in resonance computations. The origin of unphysical eigenvalues in scattering resonance computations is *spectral instability*, which is common for non-normal operators [1, 2]. Spectral instability is known to be less problematic with volume integral equations compared with formulations based on differential operators. Therefore, we proposed in [3] to use a Lippmann-Schwinger type of integral equation for removing spurious solutions in a one-dimensional setting.

In this paper, we show that it is possible to extended the approach in [3] to higher dimensions. In particular, we show that the used sorting scheme can be computed cheaply and give valuable information on the location of spurious eigenvalues. This test is motivated by spectral stability properties of the Lippmann-Schwinger formulation of the problem. The idea is then to test each computed pair and obtain an pseudospectral indicator  $\delta$ . Then we sort all computed pairs from the smallest to the largest value of  $\delta$ . Finally, we can choose a user defined tolerance  $\delta_{TOL}$ , and drop

---

<sup>1</sup>Department of Mathematics and Mathematical Statistics, Umeå University, MIT-Huset, 90187 Umeå, Sweden

<sup>2</sup>Department of Mathematics, Linnaeus University, Hus B, 35195 Växjö, Sweden

all pairs with  $\delta > \delta_{TOL}$ . In [3] we presented computations on several test cases for space dimension  $d = 1$ . The strategy was successful, since the proposed filtering scheme was able to identify physical pairs. However, the application of the ideas presented in [3] for  $d = 2, 3$  turn out to be more challenging. The effective application of these ideas in higher dimensions requires further considerations that are addressed in the current work. The new results confirm the efficiency of the proposed sorting scheme in  $\mathbb{R}^d$ ,  $d = 2, 3$ .

## 2. Electromagnetic and acoustic scattering resonances

Assume that  $\epsilon(x, \omega) = \epsilon(x_1, x_2, \omega)$  is independent of  $x_3$  and consider electromagnetic waves propagating in the  $(x_1, x_2)$ -plane. The  $x_3$ -independent electromagnetic field  $(\mathbf{E}, \mathbf{H})$  is then decomposed into transverse electric (TE) polarized waves  $(E_1, E_2, 0, 0, H_3)$  and transverse magnetic (TM) polarized waves  $(0, 0, E_3, H_1, H_2, 0)$  [4]. This decomposition reduces Maxwell's equations to one scalar equation for  $H_3$  and one scalar equation for  $E_3$ . The TM-polarized waves and the TE-polarized waves satisfy formally

$$-\Delta E_3 - \omega^2 \epsilon E_3 = 0 \quad \text{and} \quad -\nabla \cdot \left( \frac{1}{\epsilon} \nabla H_3 \right) - \omega^2 H_3 = 0, \quad (1)$$

respectively. For the scattering resonance problems,  $E_3$  and  $H_3$  are assumed to be locally integrable functions that satisfy an outgoing condition [5, 6].

Let the physical domain  $\Omega_a \subset \mathbb{R}^d$  be an open ball of radius  $a$  with boundary  $\Gamma_a$ , and let  $\Omega_r := \text{supp}(\epsilon - 1) \subset \Omega_a$  be the bounded domain defining the resonators. Hence, we assume that the relative permittivity  $\epsilon$  in  $\mathbb{R}^d \setminus \Omega_r$  is one. Furthermore, let  $\Omega_r := \cup_{i=1}^N \Omega_i$  denote the union of disjoint resonators  $\Omega_1, \Omega_2, \dots, \Omega_N$ , satisfying  $0 < \epsilon_{\min} \leq |\epsilon(x)| \leq \epsilon_{\max}$  for all  $x \in \Omega_a$ , as shown in figure 1. A *scattering resonance* was in [7] defined as a complex number  $\omega$  for which the Lippmann-Schwinger equation

$$T(\omega)u := u - K(\omega)u = 0 \quad (2)$$

has a non-zero solution  $u$ . The integral operator  $K$  in (2) is for TM/TE waves given by

$$\begin{aligned} TM: K(\omega)u &:= \omega^2 \int_{\Omega_r} \Phi(x, y) (\epsilon - 1) u \, dy \\ TE: K(\omega)u &:= \nabla \cdot \int_{\Omega_r} \Phi(x, y) \left( \frac{1}{\epsilon} - 1 \right) \nabla u \, dy \end{aligned}, \quad \Phi(x, y) := \begin{cases} \frac{i}{2\omega} e^{i\omega|x-y|}, & d = 1 \\ \frac{i}{4} H_0^{(1)}(\omega|x-y|), & d = 2. \end{cases} \quad (3)$$

Here,  $\Phi(x, y)$  is known as the outgoing Green function in free space for the Helmholtz equation [5, 6]. Notice that while we are interested in  $x \in \Omega_a$ , the integration in (2) is only performed over  $\Omega_r$ , since the integration over the air region  $\Omega_0 := \Omega_a \setminus \Omega_r$  is zero.

The scattering resonance problem (2) is a highly non-linear eigenvalue problem, where the matrices after discretization are large and full. It is possible to accurately solve the non-linear eigenvalue problem  $T(\omega)u = 0$  in  $\mathbb{R}$  using a standard laptop; see e.g. [8, 3]. However, accurate computations of eigenpairs of (2) in higher dimensions would require huge computer resources; See [9] and the discussion in Section 7.6.

### Acoustic scattering resonances in $\mathbb{R}^3$

Sound-soft materials are characterized by the speed of sound  $c(x)$  and we assume that acoustic resonators are defined by  $\Omega_r := \text{supp}(c^{-2} - 1) \subset \Omega_a$ . Then, the acoustic pressure  $u$  satisfies formally the Helmholtz equation

$$-\Delta u - \frac{\omega^2}{c(x)^2} u = 0, \quad (4)$$

where the outgoing condition can be expressed as  $u$  satisfying an expansion in spherical harmonics outside the open ball  $\Omega_a$  [10]. Moreover,  $(u, \omega)$  is a scattering resonance pair if (2) holds with

$$K(\omega)u := \omega^2 \int_{\Omega_r} \Phi(x, y) \left( \frac{1}{c(y)^2} - 1 \right) u(y) dy, \quad \Phi(x, y) = \frac{e^{i\omega|x-y|}}{4\pi|x-y|}. \quad (5)$$

Note that the acoustic problem in  $\mathbb{R}^d$ ,  $d = 1, 2, 3$  is analogous to TM-polarized electromagnetic waves with  $\epsilon = 1/c^2$ .

### 2.1. Alternative formulations

Understanding the resonance behavior of structures in unbounded domains is important and many different approaches have been proposed. Graded material properties are increasingly popular in applications [11] and we will therefore not consider boundary integral equations. However, boundary integral equation based methods are a good alternative for cases with piecewise constant coefficients and not too complicated geometry [12]. The most popular method to compute resonances in  $\mathbb{R}^d$ ,  $d > 1$  is the finite element (FE) method with a perfectly matched layer (PML). In recent years, finite element methods based on Hardy space infinite elements (HIF) [13] and DtN maps [14] have also been proposed as strong alternatives to compute resonances in higher dimensions. For the DtN map, recent developments in computational linear algebra are a key to the high performance of the method [15, 16]. Discretization with FE of the PML and HIF formulations result in sparse matrices, and a formulation in terms of a DtN result in sparse matrices except a small dense block corresponding to the DtN map. Moreover, the PML and HIF formulations result in a standard generalized eigenvalue problem if  $\epsilon$  is  $\omega$ -independent and in the general case the non-linearity in  $\omega$  is completely determined by  $\epsilon(x, \omega)$ . Hence, the PML and HIF formulations seem to have the most attractive properties of the considered methods. However, it is very important to also take into account the so called spectral instability. Then, the picture changes completely, as discussed in the next section.

### 2.2. Spectral instability and pseudospectra

Let  $A$  denote an unbounded closed linear operator in a Hilbert space with domain  $\text{dom } A$ , spectrum  $\sigma(A)$ , and resolvent set  $\rho(A)$ . Then  $A$  exhibits high *spectral instability* if for a very small  $\delta > 0$  there exist many  $\omega^2 \in \mathbb{C}$  and  $u \in \text{dom } A$  such that

$$\|(A - \omega^2)u\| \leq \delta \|u\| \quad (6)$$

even though  $\omega^2$  is not close to  $\sigma(A)$  [17]. This is closely related to the pseudospectrum  $\sigma_\delta(A)$  which is defined as the union of  $\sigma(A)$  and all  $\omega^2$  in the resolvent set  $\rho(A)$  for which it exists an  $u \in \text{dom } A$  such that (6) holds. The generalization of those results to an operator function  $T$  is straightforward and we will in some of the numerical computations rely on the following alternative characterization of the pseudospectrum:

$$\sigma_\delta(T) = \sigma(T) \cup \{\omega \in \rho(T) : \|T^{-1}(\omega)\| > \delta^{-1}\}.$$

It is well known that PML and HIF based methods encounter high spectral instability [13, 3]. Methods based on a DtN map encounter medium spectral instability [14, 3] and integral equation based methods encounter low spectral instability [3]. Hence, the Lippmann-Schwinger equation is in our setting the preferred method in terms of spectral stability. This will be further discussed in the paper.

### 2.3. Domain and material properties

In electromagnetics, the material properties of non-magnetic metals are characterized by the complex relative permittivity function  $\epsilon$ , which changes rapidly at optical frequencies  $\omega$ . The most common accurate material model is then the Drude-Lorentz model

$$\epsilon_{\text{metal}}(\omega) := \epsilon_\infty + \sum_{j=0}^{N_p} \frac{f_j \omega_p^2}{\omega_j^2 - \omega^2 - i\omega\gamma_j}, \quad (7)$$

where  $\epsilon_\infty \geq 1$  and  $f_j, \omega_p, \omega_j, \gamma_j$  are non-negative [4]. Hence, the Maxwell eigenvalue problem in the spectral parameter  $\omega$  is nonlinear for metal-dielectric nanostructures. Assume that the domain of the resonators can be written in the form  $\Omega_r := \cup_{i=1}^N \Omega_i$  and let  $\chi_{\Omega_m}$  denote the characteristic function of the subset  $\Omega_m$ . For material properties that are piecewise constant in  $\Omega_a$ , we assume a permittivity function in the form

$$\epsilon(x, \omega) := \sum_{m=0}^{N_r} \epsilon_m(\omega) \chi_{\Omega_m}(x), \quad x \in \Omega_a, \quad \omega \in \mathcal{D}, \quad (8)$$

where the dependencies on  $\omega \in \mathcal{D} \subset \mathbb{C}$  in  $\epsilon_m$  for  $m = 0, 1, \dots$  are of Drude-Lorentz type (7). In addition, we will consider graded material properties, meaning that  $\epsilon$  is a continuous function in  $x$ . In linear acoustics, the speed of sound  $c$  is assumed to be independent of the frequency.

### 3. DtN and PML based methods

In the next sections, we will describe two common approaches to compute scattering resonances and the restriction of resonance modes to a compact subset of  $\mathbb{R}^d$ . In the following, we use the notation

$$-\nabla \cdot (\rho \nabla u) - \omega^2 \eta u = 0, \quad (9)$$

where  $u := E_3$ ,  $\rho := 1$ ,  $\eta := \epsilon$  for the TM-case and  $u := H_3$ ,  $\rho := 1/\epsilon$ ,  $\eta := 1$  for the TE-case.

We define for  $u, v \in H^1(\Omega_a)$  the forms

$$\mathfrak{a}(\omega)[u, v] := \int_{\Omega_a} \rho \nabla u \cdot \nabla \bar{v} \, dx, \quad \mathfrak{b}(\omega)[u, v] := \int_{\Omega_a} \eta u \bar{v} \, dx, \quad (10)$$

where in (10),  $\rho$  and  $\eta$  are functions of  $\omega \in \mathcal{D}$ . Let  $\mathcal{Z}$  denote the set of values  $\omega$  that are zeros or poles of  $\epsilon$  and set  $\mathcal{D} := \mathbb{C} \setminus \mathcal{Z}$ .

#### 3.1. DtN based methods

Scattering resonances  $\omega$  and quasi-normal modes  $u$  restricted to  $\Omega_a$  can be determined from a problem with a Dirichlet-to-Neumann (DtN) map [18, 19, 14]. Below we present variational formulations for  $\mathbb{R}^d$ ,  $d = 1, 2$ . Formally,  $(\omega, u)$  is a scattering resonance pair if (9) holds in  $\Omega_a$  and

$$\frac{\partial u}{\partial n} = \mathcal{G}(\omega)u \quad \text{on } \Gamma := \partial\Omega_a, \quad (11)$$

where  $\partial u / \partial n$  is the normal derivative.

### 3.1.1. DtN formulation in $\mathbb{R}$

In one space dimension the scattering resonance problem restricted to  $\Omega_a := (-a, a)$  is formally: Find a non-zero  $u$  and a complex  $\omega$  such that

$$-(\rho u')' - \omega^2 \eta u = 0 \text{ for } x \in \Omega_a, \quad (12)$$

where the DtN-map at  $x = \pm a$  is

$$u'(-a) = -i\omega u(-a), \quad u'(a) = i\omega u(a). \quad (13)$$

Define for  $u, v \in H^1(\Omega_a)$  and  $\omega \in \mathcal{D} \subset \mathbb{C}$  the forms  $\mathbf{a}$ ,  $\mathbf{b}$  as in (10), and

$$g_1(\omega)[u, v] := i\omega(u(a)\bar{v}(a) + u(-a)\bar{v}(-a)). \quad (14)$$

The nonlinear eigenvalue problem is then as follows: Find vectors  $u \in H^1(\Omega_a) \setminus \{0\}$  and  $\omega \in \mathcal{D}$  satisfying

$$q_1(\omega)[u, v] := \mathbf{a}(\omega)[u, v] - \omega^2 \mathbf{b}(\omega)[u, v] - g_1(\omega)[u, v] = 0, \quad (15)$$

for all  $v \in H^1(\Omega_a)$ . Note that (15) is a quadratic eigenvalue problem if  $\epsilon$  is independent of  $\omega$  and a rational eigenvalue problem for Drude-Lorentz type of materials (7).

### 3.1.2. DtN formulation in $\mathbb{R}^2$

In this subsection, we present a DtN formulation in polar coordinates  $(r, \theta)$ . Let  $H_\nu^{(1)}(z)$  denote the Hankel function of first kind, then the DtN operator (11) on the circle  $\Gamma_a$  has the explicit form

$$\mathcal{G}(\omega)u := \frac{1}{2\pi} \sum_{\nu=-\infty}^{\infty} \omega \frac{H_\nu^{(1)'}(\omega a)}{H_\nu^{(1)}(\omega a)} e^{i\nu\theta} \int_0^{2\pi} u(a, \theta') e^{-i\nu\theta'} d\theta' \quad (16)$$

and  $\mathcal{G}(\omega) : H^{1/2}(\Gamma_a) \rightarrow H^{-1/2}(\Gamma_a)$  is bounded [18].

The resonance problem restricted to  $\Omega_a$  is formally to find non-trivial solutions  $(\omega, u)$  such that (9) and (11) with (16) holds. The theory presented in [18] can with minor changes be used in the present case to derive properties of a variational formulation of the problem.

**Variational formulation:** Let  $S$  denote the union of the set of zeros of  $H_\nu^{(1)}(\omega a)$ ,  $\nu \in \mathbb{Z}$ , and  $\mathcal{G}_{\nu_{\max}}(\omega)$  denote the operator (11) truncated after  $|\nu| = \nu_{\max}$ . The eigenvalues of the truncated version of (9)-(11) are determined by the following variational problem: Find  $u \in H^1(\Omega_a) \setminus \{0\}$  and  $\omega \in \mathcal{D} := \mathcal{D} \setminus \{\mathbb{R}^- \cup S\}$  such that for all  $v \in H^1(\Omega_a)$

$$q(\omega)[u, v] := \mathbf{a}(\omega)[u, v] - \omega^2 \mathbf{b}(\omega)[u, v] - g(\omega)[u, v] = 0, \quad (17)$$

where the forms  $\mathbf{a}$ ,  $\mathbf{b}$  are defined as in (10), and

$$g(\omega)[u, v] := (\mathcal{G}_{\nu_{\max}}(\omega)u, v)_{\Gamma_a} = \sum_{\nu=-\nu_{\max}}^{\nu_{\max}} \omega a \frac{H_\nu^{(1)'}(\omega a)}{H_\nu^{(1)}(\omega a)} \hat{u}_\nu \bar{\hat{v}}_\nu, \quad \hat{\varphi}_\nu = \frac{1}{\sqrt{2\pi}} \int_0^{2\pi} \varphi(a, \theta) e^{-i\nu\theta} d\theta. \quad (18)$$

### 3.2. PML based methods

In the previous section, a DtN-map was used to reduce the exterior Helmholtz problem to a bounded domain. In this section, we consider an alternative approach based on a complex coordinate stretching (the PML method), which results in a linear eigenvalue problem for non dispersive material coefficients [20]. The method consists on attaching to  $\Omega_a$  a buffer layer of thickness  $\ell$ , where outgoing solutions decay rapidly. The buffer domain is referred to as  $\Omega_{PML}$  and the full computational domain  $\Omega := \Omega_a \cup \Omega_{PML}$  is enlarged as shown in the Figure 1.

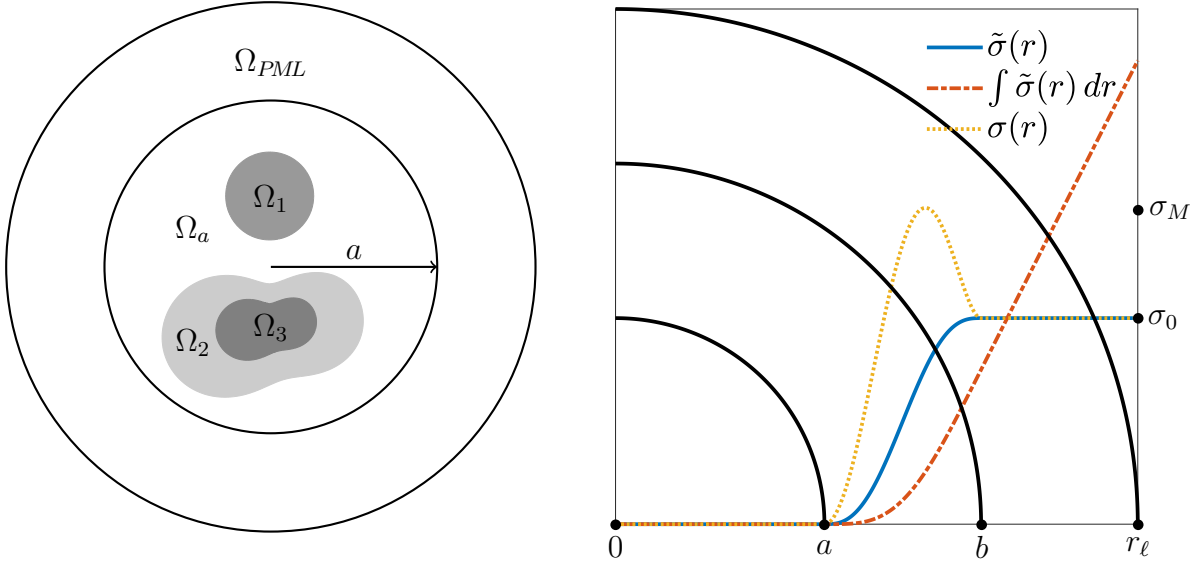


Figure 1: Left) Arbitrary configuration of resonators. Right) PML stretching function.

### 3.2.1. PML formulation in $\mathbb{R}$

Let  $\ell > 0$ , and  $0 < a < b < r_\ell$ , with  $r_\ell = b + \ell$ . The action of the PML is defined through the stretch function

$$\tilde{\sigma}(r) := \begin{cases} 0, & \text{if } r < a \\ P(r), & \text{if } a \leq r \leq b \\ \sigma_0, & \text{if } r > b \end{cases} \quad (19)$$

with  $r = |x|$ , and where the polynomial  $P(r)$  is required to be increasing in  $[a, b]$ , and  $\tilde{\sigma}(r)$  is sufficiently smooth  $C^2(0, r_\ell)$ . For this we introduce the fifth order polynomial  $P(r)$  satisfying:  $P(a) = P'(a) = P''(a) = P'(b) = P''(b) = 0$  and  $P(b) = \sigma_0$ .

The PML problem is restricted to  $(-r_\ell, r_\ell)$  and the PML strength function has then the profile shown in Fig. 1. In the following sections, we consider the complex change of variable and transformation rule

$$\tilde{x} = \int_{x_0}^x \tilde{\alpha}(y) dy, \quad \frac{d}{d\tilde{x}} = \frac{1}{\tilde{\alpha}(x)} \frac{d}{dx}, \quad \text{with } \tilde{\alpha}(x) = 1 + i\tilde{\sigma}(x), \quad (20)$$

where  $x_0 = -\infty$  in  $\mathbb{R}^-$  and  $x_0 = a$  in  $\mathbb{R}^+$ .

For finite element computations we restrict the domain to  $\Omega_\ell := (-r_\ell, r_\ell)$ , and define  $\Omega_{PML} = (-r_\ell, -a) \cup (a, r_\ell)$  and choose similarly as in [20] homogeneous Dirichlet boundary conditions. Formally, the *finite PML problem* is then: Find the eigenpairs  $(\omega, u)$  such that

$$-\frac{d}{dx} \left( \frac{\rho}{\tilde{\alpha}} \frac{du}{dx} \right) - \omega^2 \eta \tilde{\alpha} u = 0, \quad x \in \Omega_\ell, \quad u(r_\ell) = 0 \quad \text{and} \quad u(-r_\ell) = 0. \quad (21)$$

In the following, we consider a variational formulation of (21).

Find  $u \in H_0^1(\Omega_\ell) \setminus \{0\}$  and  $\omega \in \mathcal{D} := \mathbb{C} \setminus \mathcal{Z}$  such that for all  $v \in H_0^1(\Omega_\ell)$

$$t_1(\omega)[u, v] := \mathbf{a}(\omega)[u, v] - \omega^2 \mathbf{b}(\omega)[u, v] + \hat{t}_1(\omega)[u, v] = 0, \quad (22)$$

where  $\hat{t}_1(\omega)[u, v] = (\frac{1}{\tilde{\alpha}} u', v')_{\Omega_{PML}} - \omega^2 (\tilde{\alpha} u, v)_{\Omega_{PML}}$ , and the forms  $\mathbf{a}$ ,  $\mathbf{b}$  are defined as in (10).

### 3.2.2. PML formulation for $\mathbb{R}^d$

Approximation of resonances using a radial PML was analyzed in [20] and we will here only consider the PML problem truncated to the ball  $\Omega \subset \mathbb{R}^d$ ,  $d = 2, 3$ . The used complex stretching functions are as in one-dimension of the form (19). Let  $\mathcal{Z}$  denote the set of values  $\omega$  that are zeros or poles of  $\epsilon$  and let  $\Omega := \Omega_a \cup \Omega_{PML}$  denote a partition into the PML-region and the part of the domain  $\Omega_a$  containing the resonators.

In the sequel we need the following definitions

$$\begin{aligned}\tilde{\alpha}(r) &:= 1 + i\tilde{\sigma}(r), & \tilde{r}(r) &:= (1 + i\tilde{\sigma})r = \tilde{\alpha}(r)r, \\ \sigma(r) &:= \tilde{\sigma}(r) + r \frac{\partial \tilde{\sigma}}{\partial r}, & \alpha(r) &:= \frac{\partial \tilde{r}}{\partial r} = 1 + i\sigma(r),\end{aligned}\tag{23}$$

with the properties  $\sigma(r) = \partial(r\tilde{\sigma})/\partial r$  and  $\alpha(r) = \tilde{\alpha}(r) = 1 + i\sigma_0$  for  $r > b$ .

It is clear that the PML coefficients are designed such that for  $r \leq a$ , we obtain  $\sigma(r) = 0$  and  $\alpha(r) = 1$ , which is the same as  $\tilde{r} = r$ . Hence, the PML operator restricted to  $r \leq a$  corresponds to the original operator in problem (9) (no PML effect).

**Variational formulation:** The eigenvalues of (9) are then determined by the following variational problem

Find  $u \in H_0^1(\Omega) \setminus \{0\}$  and  $\omega \in \mathcal{D} := \mathbb{C} \setminus \mathcal{Z}$  such that for all  $v \in H_0^1(\Omega)$

$$t(\omega)[u, v] := \mathbf{a}(\omega)[u, v] - \omega^2 \mathbf{b}(\omega)[u, v] + \hat{t}(\omega)[u, v] = 0,\tag{24}$$

where  $\hat{t}(\omega)[u, v] := (\mathcal{A}\nabla u, \nabla v)_{\Omega_{PML}} - \omega^2 (\mathcal{B}u, v)_{\Omega_{PML}}$ , and the forms  $\mathbf{a}$ ,  $\mathbf{b}$  are defined as in (10).

As an example for  $d = 2$ , direct transformation of (24) from polar to Cartesian coordinates results in

$$\mathcal{A} = \begin{pmatrix} \frac{\tilde{\alpha}}{\alpha} \cos^2 \theta + \frac{\alpha}{\tilde{\alpha}} \sin^2 \theta & \left( \frac{\tilde{\alpha}}{\alpha} - \frac{\alpha}{\tilde{\alpha}} \right) \sin \theta \cos \theta \\ \left( \frac{\tilde{\alpha}}{\alpha} - \frac{\alpha}{\tilde{\alpha}} \right) \sin \theta \cos \theta & \frac{\tilde{\alpha}}{\alpha} \sin^2 \theta + \frac{\alpha}{\tilde{\alpha}} \cos^2 \theta \end{pmatrix}, \quad \mathcal{B} := \alpha \tilde{\alpha}.\tag{25}$$

Even though  $\mathcal{A}$ , and  $\mathcal{B}$  are defined in the whole  $\Omega$ , their action takes place only in  $\Omega_{PML}$ .

## 4. Discretization of the Lippmann-Schwinger equation

In this section we present a collocation method for discretization of the Lippmann-Schwinger equation (2), which will be used to compute resonances in one-dimension and is the base for the numerical sorting algorithm in Section 6. Further computational details are given in Section 7.6.

### 4.1. A Galerkin-Nyström method

We present a Galerkin-Nyström discretization method for linear Fredholm integral equations of the second kind, with kernels satisfying  $\int_D \int_D |\Phi(x, y)|^2 dx dy < \infty$  for  $x, y$  in the compact set  $D \subset \mathbb{R}^d$ . In [21], this method is referred to as case (A) of the Galerkin methods, and convergence for the problem with sources is also discussed. In [7, Sect. 3.2] the method was used for resonance computations for  $d = 2$ .

Let  $\{\varphi_j\}_{j=1}^N$  be piecewise polynomial functions with the property  $\varphi_j(x_i) = \delta_{ji}$ ,  $\{x_i\}_{i=1}^N \in \Omega_a$ . We introduce the representation  $u^\gamma = \sum_j^N \xi_j \varphi_j$ , and with the use of (2) we obtain the nonlinear

eigenvalue problem: Find  $\xi \in \mathbb{C}^N$  and  $\omega^\gamma \in \mathbb{C}$  such that

$$\begin{aligned} T^\gamma(\omega^\gamma)\xi &= (I - K(\omega^\gamma))\xi = 0, \text{ with} \\ TM : K_{ij}(\omega) &:= \omega^2 \int_{\Omega_r} \Phi(x_i, y) (\epsilon - 1) \varphi_j dy, \\ TE : K_{ij}(\omega) &:= \nabla \cdot \int_{\Omega_r} \Phi(x_i, y) \left(\frac{1}{\epsilon} - 1\right) \nabla \varphi_j dy, \end{aligned} \quad (26)$$

The Nyström method consists in choosing the collocation points  $x_i$  as the nodes of a high order quadrature rule. By doing this, the convergence of the scheme is considerably improved. In Section 7.6 we describe some of the implementation details of the Galerkin-Nyström discretization.

The resulting nonlinear matrix eigenvalue problem (26) is solved by using a contour integration based method [22, 23, 24].

**Remark 1.** *The formulation in (2) uses information of the exact solution of the problem at every discretization node  $x_i$ , through its fundamental solution  $\Phi(x, y)$ . From where the numerical scheme is flexible in the way that it can be posed in the smallest domain  $\Omega_r$ , as well as in larger domains  $\Omega \supset \Omega_r$ , without taking any special treatment for boundary conditions.*

## 5. FE discretization of the DtN and PML based formulations

In this section we discuss briefly the details involved in the assembly of the matrices corresponding to the discretization of the formulations given in (9), and (2).

### 5.1. Discretization with the finite element method

Let the domain  $\Omega \subset \mathbb{R}^d$  be covered with a regular and quasi uniform finite element mesh  $\mathcal{T}(\Omega)$  consisting of elements  $\{K_j\}_{j=1}^N$ . The mesh is designed such that the permittivity function  $\epsilon$  is continuous in each  $K_j$ . Let  $h_j$  be the length of the largest diagonal of the non-curved primitive  $K_j$  and denote by  $h$  the maximum mesh size  $h := \max_j h_j$ .

Let  $\mathcal{P}_p$  denote the space of polynomials on  $\mathbb{R}^d$  of degree  $\leq p$  and define the  $N$  dimensional finite element space

$$S^\gamma(\Omega) := \{u \in H^1(\Omega_a) : u|_{K_j} \in \mathcal{P}_p(K_j) \text{ for } K_j \in \mathcal{T}\}. \quad (27)$$

The computations of discrete resonance pairs  $(u^\gamma, \omega^\gamma)$  are for  $d = 2, 3$  performed in the approximated domain  $\Omega^\gamma$  using curvilinear elements [25]. The meshes used are *shape regular* in the sense of [26, Sec. 4.3], and consist of quadrilateral/brick elements with curvilinear edges/surfaces that deviate slightly from their *non-curved* primitives.

### 5.2. Assembly of the FE matrices

In this section we refer to domains  $\Omega_q \in \mathbb{R}^d$ . Let  $\{\varphi_1, \dots, \varphi_N\}$  be a basis of  $S^\gamma(\Omega^\gamma)$ . Then  $u_\gamma \in S^\gamma(\Omega^\gamma)$ , and the entries in the finite element matrices are of the form

$$u_\gamma = \sum_{j=1}^N \xi_j \varphi_j, \quad A_{ij} = (\rho \nabla \varphi_j, \nabla \varphi_i)_{\Omega_a^\gamma}, \quad M_{ij} = (\eta \varphi_j, \varphi_i)_{\Omega_a^\gamma}. \quad (28)$$

The matrix eigenvalue problem is then: Find the eigenpairs  $(\omega, \xi) \in \mathcal{D} \times \mathbb{C}^N \setminus \{0\}$  such that

$$F(\omega) \xi := (A - \omega^2 M + Q)(\omega) \xi = 0, \quad (29)$$



where the corresponding matrix valued function is

$$Q_{ij}(\omega) := \begin{cases} -g_1(\omega)[\varphi_j, \varphi_i], & \text{DtN and } d = 1 \\ -g(\omega)[\varphi_j, \varphi_i], & \text{DtN and } d = 2 \end{cases}, \text{ or } \begin{cases} \hat{t}_1(\omega)[\varphi_j, \varphi_i], & \text{PML and } d = 1 \\ \hat{t}(\omega)[\varphi_j, \varphi_i], & \text{PML and } d = 2, 3 \end{cases}. \quad (30)$$

In the case where  $\epsilon(\omega, x)$  is given as piecewise smooth function of space, we write (29) as

$$F(\omega) \xi := \left( \sum_{m=0}^{N_r} \{ \rho_m(\omega) \tilde{A}_m - \omega^2 \eta_m(\omega) \tilde{M}_m \} + Q(\omega) \right) \xi = 0, \quad (31)$$

with matrices  $\tilde{A}_{ij}^m = (\nabla \varphi_j, \nabla \varphi_i)_{\Omega_m^\gamma}$ ,  $\tilde{M}_{ij}^m = (\varphi_j, \varphi_i)_{\Omega_m^\gamma}$ ,  $m = 0, 1, \dots, N_r$ .

**Remark 2. Truncation of the DtN:** Let  $\lceil z \rceil$  be the smallest integer greater than or equal to  $z$ . We use the rule  $\nu_{\max} = \lceil a \omega_M \rceil$  according to the results in [14], where from the considered spectral window,  $\omega_M$  is the largest real part allowed for computations of eigenvalues.

**Remark 3. Truncation of the PML:** The PML is set up following the discussions in [20, 3], which accounts for large enough  $\ell$  and  $\sigma_0$  such that the search region is feasible. Additionally, we use the space  $S_0^\gamma(\Omega) := \{u \in S^\gamma(\Omega) : u = 0 \text{ for } x \in \partial\Omega^\gamma\}$  for computations with the PML formulation.

Finally, we mention that all discretization methods presented in this work use the same FE space over  $\Omega_a$ .

**Remark 4.** All formulations (LS, DtN, PML) use the FE triangulation  $\mathcal{T}(\Omega_a)$ , which is the restriction of  $\mathcal{T}(\Omega)$  to  $\Omega_a$ .

By using the FE mesh suggested in Remark 4, we ensure that the approximation properties in the physical domain are the same for all formulations.

## 6. Numerical sorting of resonances

In this section we derive a discrete form of (2) that allow us to identify resonances from spurious solutions once we have computed FE solutions  $(\omega_m^\gamma, u_m^\gamma)$  to (29) or to (31). The resulting expression for the sorting scheme is a discrete form of the condition  $\|\chi_a T(\omega) \chi_a u\| < \delta$ , where  $u^\gamma$  is a FE solution restricted to  $\Omega_a$ . Let  $\{\varphi_j\}$  be a basis for  $S^\gamma(\Omega_a)$  and let  $P^\gamma$  be the  $L_2$ -projection on  $S^\gamma(\Omega_a)$ . Then, the discrete Lippmann-Schwinger equation (26) is written in the form

$$T(\omega)u^\gamma = u^\gamma - K(\omega)u^\gamma, \quad u^\gamma := \sum_{j=1}^N \xi_j \varphi_j, \quad \text{with } \|u^\gamma\|_{L^2(\Omega_a)} = 1.$$

**Definition 5. Pseudospectrum indicator:** The computed eigenvalue  $\omega^\gamma$  belongs, for given  $\delta > 0$ , to the  $\delta$ -psudospectrum  $\sigma_\delta(T^\gamma)$  if the pair  $(\omega^\gamma, u^\gamma)$  satisfies  $\|T^\gamma(\omega^\gamma)u^\gamma\|_{\Omega_a} < \delta$ . Then, for a given domain  $\Omega_a \supseteq \Omega_r$ , we define the pseudospectrum indicator as

$$\delta^\gamma(\Omega_a) := \|T^\gamma(\omega^\gamma)u^\gamma\|_{\Omega_a}. \quad (32)$$

Particularly, we want to be able to measure whether the computed eigenpair  $(\omega^\gamma, u^\gamma)$  is converging to a physical pair. Naturally, non convergent pairs exhibit large  $\delta^\gamma$  values.

Additionally, we have that certain spurious eigenpairs introduced by using the PML method are easily identified and can be removed by using the following definition.

**Definition 6. PML added eigenpairs:** *The use of the coordinate stretching technique in formulations (22), (24) introduces new eigenpairs to problem (9). These new eigenvalues accumulate close to the critical line of the modified PML problem [3], and eigenfunctions  $v_m$  exhibit oscillations in  $\Omega_{PML}$ , but decay in the physical region  $\Omega_a$ . Then, by using the normalization  $\|v_m\|_{L^2(\Omega)} = 1$ , the PML critical eigenvalues exhibit*

$$0 < \frac{\|v_m\|_{L^2(\Omega_a)}}{|\Omega_a|} < \frac{\|v_m\|_{L^2(\Omega_{PML})}}{|\Omega_{PML}|},$$

*which can be successfully used as a filtering criterion for removing PML added eigenpairs.*

## 7. Computational details

In this section we outline the computational details for the FE discretization of the DtN and PML based formulations in Section 5. Furthermore, we present results on integration of weakly singular kernels that are used in the new numerical sorting scheme in Subsection 7.7. For convenience of the reader we provide a summary of the used standard techniques.

### 7.1. Master element and transfinite interpolation

Consider a physical element  $K$  and let  $\mathcal{K} := (-1, 1)^d$  denote the master element. Numerical quadrature is used to integrate a function over  $K$  and when high order polynomial spaces are used, it is convenient to compute information from the shape functions  $\varphi_j, \nabla\varphi_j$  in the master element  $\mathcal{K}$  and then store it. In this way we gain in performance as computations from high polynomials are expensive. Consequently, functions defined over a physical element  $K$  are mapped to functions over  $\mathcal{K}$ , where we perform integration. Then, the mapping  $X_K : \mathbb{R}^d \rightarrow \mathbb{R}^d$  transforms coordinates as  $K = X_K(\mathcal{K})$ . The action of the mapping is enforced by the Jacobian's determinant  $J = \det(DX_K)$  [27, Sec. 3.3], [28, Sec. 3.4]. Then, we have

$$\int_K f(x) dx = \int_{\mathcal{K}} f \circ X_K(y) J(y) dy. \quad (33)$$

For the case where  $K$  is a line, quadrilateral or a brick element, the explicit expression for  $X_K(\mathcal{K})$  is a known bilinear transformation. When  $K$  has curved edges,  $X_K(\mathcal{K})$  can be described by the so-called theory of Transfinite Interpolation [29], and the implementation and computational details can be found in [30], [28, Sec. 3.2]. A general rule of thumb is that the bending of the edges must be small compared to the diameter of the element, and that the angles at the element corners should be close to  $\pi/2$ . For further details and explicit error estimates on curved elements the reader is referred to [27, Sec. 3.3], [31, Sec. 6.7]. For the description on how  $\varphi_j, \nabla\varphi_j$  transform from  $K$  to  $\mathcal{K}$ , and other related details, the reader is referred to [28, Sec. 3.3].

## 7.2. Evaluation of integrals

In this subsection, we revise briefly numerical integration by *Gaussian-Legendre* quadratures. In the one dimensional case, integration over the master element is approximated by formulas of the form  $\int_{\mathcal{K}} f(x) dx = \sum_{i=1}^m w_i f(x_i) + E$ , where  $w_i$  are the quadrature weights,  $x_i$  the quadrature nodes, and  $E$  is the quadrature error or remainder. The coefficients  $w_i$  are all positive [32, Sec. 8.4]. These type of quadrature rules are derived under the assumption that  $f \in C^{2m}(\mathcal{K})$ ,  $m \in \mathbb{N}$ , then, the Weierstrass approximation theorem [32, Sec 1.2] guarantees the existence of a polynomial  $P(x)$  such that  $\sup_{x \in \mathcal{K}} |f(x) - P(x)| \leq \delta$ , for an specified  $\delta > 0$ . In this way  $w_i, x_i$  can be set to minimize  $E$ , and  $P(x)$  is integrated exactly. The effective way of reducing  $\sup_{x \in \mathcal{K}} |f(x) - P(x)|$  is by increasing the polynomial degree  $p$  until the residual is below  $\delta$ . In the quadrature formula, increasing  $p$  is equivalent to increasing the number of evaluation points  $m$ . The remainder for the  $m$ -point Gaussian quadrature satisfies

$$|E| \leq C |f^{(2m)}(\xi)|, \text{ for } \xi \in \mathcal{K}, \quad (34)$$

where we see that if  $f$  is a polynomial of order  $p < 2m$ , the remainder vanishes and the quadrature gives the exact integral value. Further details on Gaussian quadratures can be revised in e.g. [32, Ch. 8], and implementation details are provided in [33, Ch 4].

In  $\mathbb{R}^d$ ,  $d > 1$ , we describe quadrature formulas for integration of  $f \in C^{2m}(\mathcal{K})$ , when a physical element  $K$  is allowed to be curved. Then, we resource to the formula

$$\int_K f(x) dx = \int_{\mathcal{K}} f \circ X_K(y) J(y) dy = \sum_{j=1}^{m^2} w_j f(\mathbf{x}_j) + E(K), \quad (35)$$

where the new weights and nodes  $w_j, \mathbf{x}_j$  are the piled up tensor product version of vector of the corresponding one dimensional values. For example, with  $d = 2$ , and  $i, j = 1, 2, \dots, m$ , the new index is  $k = (i-1)m + j$ , and  $y_k = [y_i, y_j]^T$ . Then, we obtain the transformed nodes  $\mathbf{x}_k = X_K(y_k)$  and the corresponding weights as  $w_k = w_i w_j J(y_k)$ .

Finally, we discuss the composite of a quadrature rule, when integration is performed over a domain  $\Omega \supseteq \cup_i K_i$  defined by the union of several elements  $K_i$ . The integrand is now required to be piecewise smooth  $f \in C^{2m}(K_i)$ , for  $i = 1, 2, \dots, N_{\text{elements}}$ . Then, we obtain

$$\int_{\Omega} f(x) dx = \sum_i \int_{K_i} f(x) dx = \sum_i \sum_k w_k(K_i) f(\mathbf{x}_k(K_i)) + E(\Omega), \quad (36)$$

where for each element  $K_i$ , we have the quadrature pairs  $\mathbf{x}_k(K_i), w_k(K_i)$ , similarly as in (35).

The polynomial spaces that we use for  $d = 2, 3$  are based on the tensor product of one dimensional finite element spaces [33, Sec. 2.2], [34]. As we work with piecewise smooth coefficients, we make sure that the jumps of  $f$  coincide with the possibly curved element edges  $\partial K_i$ , such that for  $\mathbf{x} \in K_i$  we have  $f \in C^{2m}(K_i)$ . This allow us to use quadrature rules in each individual element and guarantee convergence of the error of the numerical integration.

### 7.2.1. Integrating weakly singular kernels

In the discretization of the Lippmann-Schwinger formulation (26), we encounter the situation where the integrand will contain both evaluation points  $x, y$  in an element  $K_l \subset \Omega_r$ . For one-dimensional problems ( $d = 1$ ), the kernel  $\Phi(x, y)$  is continuous, but has a jump in the derivative

at points  $x = y$ . In the troublesome element  $K_l := (x_l, x_{l+1})$ , we can always split the integration interval  $K_l \rightarrow (x_l, x_j) \cup (x_j, x_{l+1})$  and perform two separate quadrature integrations. Then, by using Gauss-type of quadratures, it is possible to avoid the evaluation of  $\Phi(x_j, x_j)$  [3].

In higher dimensions ( $d = 2, 3$ ) the kernel is weakly singular [35, Sec. 2.3], what makes the integration in (26) more demanding. This difficulty can be overcome by specializing the quadratures as done for example in [36], [37], and [38]. There, extra effort was spent in refining adaptively on elements  $K_l$ , where the integrand is unbounded. Then a Nyström type of high order quadratures, combined with interpolation in polar coordinates along with other techniques were used in order to keep  $E(\Omega_r)$  small to desired order. As expected, the challenge becomes more pronounced in higher dimension as can be seen in [37] and in [38]. In those papers the aim was to solve a scattering problem through the Lippmann-Schwinger formulation for a given incoming wave. However, our case is very different as we look for scattering resonances, where the corresponding eigensolver is computationally much more demanding than a linear solve.

### 7.3. Solution of the nonlinear eigenvalue problems

The approximation of resonances based on the DtN formulation for  $d = 2$  leads to the matrix problem in (29). The solution of this NEP is based on the solution strategy presented in [14], where we use a specialization of the Infinite Arnoldi method [39, 40] called the tensor infinite Arnoldi method (TIAR). In particular we introduce a pole cancellation technique in order to increase the radius of convergence for computation of eigenvalues that lie close to the poles of the matrix-valued function.

For the approximation of resonances when the permittivity function is described by the rational model (7), we prefer to solve the corresponding matrix NEP by the techniques presented in [41], which is a specialization of the solver in [42] implemented in the SLEPc library [43].

### 7.4. Properties of volume integral equations for resonance computation

We discretize *volume* integral equations by using the scheme presented in (26), which does not require any boundary conditions as mentioned in Remark 1. In Section 8.2 we will numerically show the desired stability of the spectrum of the resulting discrete operator for perturbations of  $a$ .

**Remark 7.** *The resulting system matrices has dimensions comparable to FE matrices:  $N_l \times N_l$ , with  $N_l \leq ch^{-d}$ . However, the matrices are dense ( $\mathcal{O}(N_l^2)$  storage), non-symmetric, and the elements of  $T(\omega)$  are transcendental functions of  $\omega$ .*

The consequences of Remark 7 in a NEP solution strategy is that the matrix  $T(\omega_j)$  from (26) must be re-assembled for each new iteration  $\omega_{j+1} = \omega_j + \delta\omega$ , which is very expensive especially for problems of dimension  $d > 1$ .

### 7.5. Memory requirements

Let  $n_c$  be the number of cells in a triangulation in space dimension  $d$ ,  $p$  the polynomial degree of the basis functions in use, and  $w = 16$  bytes is the memory required to store a complex number in double precision. Given the number of non zeros elements  $N_z$  in a matrix, the memory required to store it is  $W = N_z \times w$ .

In the collocation method given in Sec. 4.1, matrices are dense and we get  $N_z^D \approx [n_c \times p^d]^2$ . In turn, the FE matrices from Sec. 5.2 are sparse, and each cell in the triangulation contributes with a block of size  $[(p+1) \times (p+1)]^d$  support points. Additionally, we have scattered connections

$d$	$p$	$m$	$n_c$	$N_z^S$	$N_z^D$	$W^S(\text{bytes})$	$W^D(\text{bytes})$
1	2	10	$10^1$	$9.0 \times 10^1$	$4.0 \times 10^2$	$1.4 \times 10^3$	$6.4 \times 10^3$
2	2	10	$10^2$	$8.1 \times 10^3$	$1.6 \times 10^5$	$1.3 \times 10^5$	$2.6 \times 10^6$
3	2	10	$10^3$	$7.3 \times 10^5$	$6.4 \times 10^7$	$1.2 \times 10^7$	$1.0 \times 10^9$
1	2	$10^2$	$10^2$	$9.0 \times 10^2$	$4.0 \times 10^4$	$1.4 \times 10^4$	$6.4 \times 10^5$
2	2	$10^2$	$10^4$	$8.1 \times 10^5$	$1.6 \times 10^9$	$1.3 \times 10^7$	$2.5 \times 10^{10}$
3	2	$10^2$	$10^6$	$7.3 \times 10^8$	$6.4 \times 10^{13}$	$1.2 \times 10^{10}$	$1.0 \times 10^{15}$
1	2	$10^3$	$10^3$	$9.0 \times 10^3$	$4.0 \times 10^6$	$1.4 \times 10^5$	$6.4 \times 10^7$
2	2	$10^3$	$10^6$	$8.1 \times 10^7$	$1.6 \times 10^{13}$	$1.3 \times 10^9$	$2.6 \times 10^{14}$
3	2	$10^3$	$10^9$	$7.3 \times 10^{11}$	$6.4 \times 10^{19}$	$1.2 \times 10^{13}$	$1.0 \times 10^{21}$

Table 1: *Memory consumption estimation for matrices in (29), and (26) for  $d = 1, 2, 3$ .*

of order  $(p+1)^d$  with neighboring cells that we omit for simplicity. A simple estimation gives  $N_z^S \approx n_c \times (p+1)^{2d}$ . Furthermore, by assuming  $m$  the division in a one dimensional partition, it is reasonable to have  $n_c = m^d$ , and  $m = 10, 10^2, 10^3$  for a small, moderate and large problem respectively.

We list our simple estimations in table 1 for  $p = 2$ , for both FE discretization methods 5.2 and collocation methods for volume integral equations 4.1. As expected, dealing with FE matrices is a standard way of discretizing wave problems and results in manageable sparse matrices for current computer memory constraints. It is evident that the load becomes larger with higher space dimension and number of cells, from where matrices for  $d = 3$  can be stored only for small and moderate problems. In the case of matrices from the collocation strategy in (26), we conclude that storage becomes computationally unfeasible in higher space dimensions, for moderate and large problems. Additionally, working with higher polynomial degree rules out even small problems.

#### 7.6. Computational platform and details

All numerical experiments have been carried out using the finite element library *deal.II* [34] with Gauss-Lobatto shape functions [33, Sec. 1.2.3]. For fast assembly and computations with complex numbers the package PETSc [44] is used.

The computational platform was provided by the High-Performance Computing Center North (HPC2N) at Umeå University, and all experiments were run on the distributed memory system Abisko. The jobs were run in serial on an exclusive node: during the process, no other jobs were running on the same node. Node specifications: four AMD Opteron 6238 processors with a total of 48 cores per node.

#### 7.7. Computational details of the sorting scheme

In order to evaluate the sorting scheme, we are interested in computing the integrals from (26) as accurately as possible. The available FE machinery for computing integrals over  $\Omega_0$ , facilitates the numerical integration, which is done similarly as described in Section 7.2.

Due to the growth of most resonant modes, the point-wise residual  $|(T^\gamma(\omega^\gamma)u^\gamma)(x_j)|$  is expected to be larger for  $x_j \in \Omega_a$ . Additionally, as discussed in Section 7.2.1, due to the unboundness of  $\Phi(x_j, x_j)$ , the computation of (26), and (32) for  $x_j \in \Omega_r$  requires considerable more effort compared to its evaluation for  $x_j \in \Omega_0$ . The apparent reason for this is that for  $x_j \in \Omega_r$  and  $d > 1$ ,

we have to numerically compute an integral with a weak singularity, which we discuss further in Section 7.2.1.

Below, we write explicitly the steps involved in computing  $\delta^\gamma(\Omega_a)$  from definition 5. First, we split the integration into separate parts over  $\Omega_0, \Omega_r$  and use the composite quadrature rules (36) for evaluating the integrals. We need the following definitions.

**Definition 8.** Let  $\mathcal{K}_0 := \{i : K_i \subset \Omega_0\}$  and  $\mathcal{K}_r := \{i : K_i \subset \Omega_r\}$  be index sets defined over  $\Omega_0$  and  $\Omega_r$ , respectively. We define the sets  $\mathcal{X}_0 := \cup_{i \in \mathcal{K}_0} \{x_j \in K_i\}_{j=1}^{m^2}$ ,  $\mathcal{X}_r := \cup_{i \in \mathcal{K}_r} \{x_j \in K_i\}_{j=1}^{m^2}$ , and denote by  $\mathcal{I}_0, \mathcal{I}_r$  the resulting extracted index sets from the new ordering.

Then, we have

$$\begin{aligned} \delta^\gamma(\Omega_a)^2 &= \|T^\gamma(\omega^\gamma)u^\gamma\|_{\Omega_a}^2 \\ &= \int_{\Omega_0} |(T^\gamma(\omega^\gamma)u^\gamma)(x)|^2 dx + \int_{\Omega_r} |(T^\gamma(\omega^\gamma)u^\gamma)(y)|^2 dy \\ &= \sum_{l \in \mathcal{K}_0} \sum_j w_j \alpha_{lj}^2 + \sum_{m \in \mathcal{K}_r} \sum_j w_j \beta_{mj}^2 + E(\Omega_0) + E(\Omega_r), \end{aligned} \quad (37)$$

where  $\alpha_{lj} := |(T^\gamma(\omega^\gamma)u^\gamma)(x_j(K_l))|$ ,  $\beta_{mj} := |(T^\gamma(\omega^\gamma)u^\gamma)(y_j(K_m))|$ , for  $x_j \in \Omega_r, y_j \in \Omega_0$ . From (26), the evaluation of  $T(\omega)u$  involves an integration over  $\Omega_r$ , which we refer to as *inner loop*. Then, for each  $j$  in  $\alpha_{lj}, \beta_{mj}$  we compute an inner loop, which is added to the explicit integration shown in (37).

#### 7.7.1. Computational costs

In this subsection, we estimate the computational cost for performing the operations involved in (37). Computationally, the errors in (37) require special treatment as discussed in 7.2.1. However, for simplicity of the estimations, we disregard additional costs from integration of weakly singular kernels in higher dimensions.

We estimate the costs in terms of the evaluation of  $u^\gamma(x_j)$  and  $\Phi(x_i, x_j)$  in complex double precision, which combined account for the heaviest work load in each individual term of (37). The evaluation of these two operations account for a rough computational time of around  $t_q \approx 10^{-6}s$  benchmarked on the processor Intel Core i7-3770, CPU: 3.40GHz.

For the estimation, assume that we have  $n_c$  cells  $K_i \subset \Omega_a$  and choose a finite element space of degree  $p$ . Then, we have  $n_c \times (p+1)^d$  terms in the outer loop and the inner loop requires  $n_r \times (p+1)^d$  terms, where  $n_r$  denotes the number of cells in  $\Omega_r$ .

Hence, computing  $\|T^\gamma(\omega^\gamma)u^\gamma\|_{\Omega_a}^2$  costs about  $n_c \times (p+1)^d \times n_r \times (p+1)^d = n_c \times n_r \times (p+1)^{2d}$  evaluations of the kernel.

Assume  $m$  as the size of a one dimensional partition, from where it is reasonable to have  $n_r = m^d, n_c = (cm)^d$ , for  $c > 1$ . Then, the cost is given by  $c^d \times (m \times (p+1))^{2d}$ , which becomes prohibitively expensive for higher dimensions.

As an illustration, we can check estimations for the cost, inner time  $t_i$ , total time  $t$  running on a single processor. We use  $c = 2$ , and it is reasonable to use  $m = 10, 10^2, 10^3$  for a small, moderate and large problem respectively. In Table 2 we show the estimations for the computational costs and times required by (37), with the aim of getting a better intuition of the requirements of the computation.

The presented sorting scheme is fully parallelizable and the total time of execution can be reduced by a factor of ten by using additional cores. However, the conclusion of Table 2 is that the computational cost is extremely high for realistic computations. Basically, evaluating  $\delta_m^\gamma(\Omega_a)$  as in (32) results in sorting schemes that are far more expensive than the solution of the NEP (29).

$d$	$p$	$m$	$n_r$	cost	$t_i(s)$	$t(s)$
1	2	$10^1$	$10^1$	$1.8 \times 10^3$	$9.0 \times 10^{-5}$	$1.8 \times 10^{-3}$
2	2	$10^1$	$10^2$	$3.2 \times 10^6$	$8.1 \times 10^{-3}$	$3.2 \times 10^0$
3	2	$10^1$	$10^3$	$5.8 \times 10^9$	$7.3 \times 10^{-1}$	$5.8 \times 10^3$
1	2	$10^2$	$10^2$	$1.8 \times 10^5$	$9.0 \times 10^{-4}$	$1.8 \times 10^{-1}$
2	2	$10^2$	$10^4$	$3.2 \times 10^{10}$	$8.1 \times 10^{-1}$	$3.2 \times 10^4$
3	2	$10^2$	$10^6$	$5.8 \times 10^{15}$	$7.3 \times 10^2$	$5.8 \times 10^9$
1	2	$10^3$	$10^3$	$1.8 \times 10^7$	$9.0 \times 10^{-2}$	$1.8 \times 10^2$
2	2	$10^3$	$10^6$	$3.2 \times 10^{14}$	$8.1 \times 10^1$	$3.2 \times 10^8$
3	2	$10^3$	$10^9$	$5.8 \times 10^{21}$	$7.3 \times 10^5$	$5.8 \times 10^{15}$

Table 2: Cost and time estimation for computing (37) for  $d = 1, 2, 3$ .

### 7.7.2. Sorting strategy

A pseudospectrum strategy based on Definition 5, consist of the sorting of computed pairs  $(\omega_m^\gamma, \xi_m)$ , solution to (29), according to their respective indicator  $\delta_m^\gamma(\Omega_a)$ . As discussed in Section 7.2.1, the evaluation of the  $\beta_{mj}$  in (37) requires special treatment such as non-standard quadrature rules similar to the ones introduced in [36, 37, 38]. Additionally, as estimated in Sec. 7.7.1 and Table 2, the evaluation of  $\delta_m^\gamma(\Omega_a) := \|u_m - Ku_m\|_{L^2(\Omega_a)}$  in higher dimensions is prohibitively expensive because  $Ku_m$  is a volume integral operator. With these issues in mind, our aim is to propose an approximated version of  $\delta^\gamma(\Omega_a)$  from definition 5 such that we improve in performance compared to the results in Table 2, and we avoid the use of specialized quadrature schemes for the evaluation of singular kernels. Then, our goal is to reduce the complexity of the sorting scheme, such that the new strategy becomes at most as expensive as the computation of the inner loop, which is a reasonable price to pay.

In the remaining of the section, we present an alternative sorting alternative based on Definition 5 with computational cost that scales with the cost of evaluating the inner loop.

### 7.7.3. Sorting estimations

The definitions given in Def. 8 are used to order quadrature pairs over elements, into two ( $q = 0, r$ ) final collection pairs that we write as  $\{x_k^q, w_k^q\} := \cup_{i \in \mathcal{K}_q} \{x_j(K_i), w_j(K_i)\}_{j=1}^{m^2}$ , and  $k \in \mathcal{I}_q$ .

Then, from the definition 5 and (37) we have

$$\begin{aligned}
\delta^\gamma(\Omega_a)^2 &= \|T^\gamma(\omega^\gamma)u^\gamma\|_{\Omega_a}^2 \\
&\approx \sum_{l \in \mathcal{K}_0} \sum_j w_j \alpha_{lj}^2 + \sum_{m \in \mathcal{K}_r} \sum_j w_j \beta_{mj}^2 \\
&\leq \max_{l \in \mathcal{I}_0} (\alpha_l)^2 \sum_{j \in \mathcal{I}_0} w_j^0 + \max_{m \in \mathcal{I}_r} (\beta_m)^2 \sum_{j \in \mathcal{I}_r} w_j^r \\
&= \max_{l \in \mathcal{I}_0} (\alpha_l)^2 \cdot |\Omega_0| + \max_{m \in \mathcal{I}_r} (\beta_m)^2 \cdot |\Omega_r|,
\end{aligned} \tag{38}$$

where  $\alpha_l := |(T^\gamma(\omega^\gamma)u^\gamma)(x_l)|$ ,  $x_l \in \mathcal{X}_0$ , and  $\beta_m := |(T^\gamma(\omega^\gamma)u^\gamma)(x_m)|$ ,  $x_m \in \mathcal{X}_r$ . In the estimate (38), we used the properties that the quadrature weights  $w_m$  are positive, and that  $|\Omega| = \int_\Omega dx = \sum_i w_i + E(\Omega)$ .

Then, (38) suggests an alternative strategy as an approximation of the pseudospectrum indicator in 5. The result is an effective and inexpensive way of testing the computed pair  $(\omega^\gamma, \xi)$ , where the cost scales linearly with the inner loop. We base our sorting strategy in the following definition.



**Definition 9. Sorting indicator:** For a given eigenpair  $(\omega_m^\gamma, v_m^\gamma)$ , and  $l_m, c > 0$ , we define the feasible sampling set  $X_m := \{x \in \Omega_0 : \inf_{y \in \Omega_r} |x - y| > l_m \text{ and } |v_m(x)| > c\}$ , and set

$$\tilde{\delta}_m := \max_{x \in X_m} \tilde{\delta}_m(x), \text{ with } \tilde{\delta}_m(x) := |v_m(x) - Kv_m(x)|. \quad (39)$$

Due to the rapid growth of eigenfunctions, we expect that non-convergent/spurious pairs exhibit  $\beta_m < \alpha_l$ . Then, for identification of spurious pairs, it is convenient to compute first the  $\alpha_l$ , as suggested in Def. 9.

**Remark 10.** The proposed strategy consists in evaluating the residual  $|(T^\gamma(\omega^\gamma)u^\gamma)(x)|$  in points  $x \in X_m$  as suggested by (39) and typically stopping after  $N_s \approx 10$  scattered evaluations is enough for practical computations. Additionally, we want to exclude points  $x_l$ , such that  $|u^\gamma(x_l)| \approx 0$ , and we want to avoid integrating over cells with a singular kernel. For this, we select points  $x_j \notin \Omega_r$  such that  $\inf_{y \in \Omega_r} |x_j - y| \geq l_m$ , in order to avoid the singularity peak. Consecutively, we select  $l_m$  such that  $|\Phi(\omega_m l_m)| \leq C_1$ , which guarantees that the integrand is bounded. Ultimately, we use the normalization  $v_m := u_m / \|u_m\|_\Omega$ , with  $\Omega := \Omega_a \cup \Omega_{PML}$  for the PML formulations. Then, we filter out added PML eigenvalues described in Def. 6 by demanding the condition  $\|v_m(x)\|_{\Omega_a} / |\Omega_a| > \|v_m\|_{\Omega_{PML}} / |\Omega_{PML}|$ .

### 7.8. Alternative strategies

The identification of spurious pairs from resonance computations has been attempted before in the literature. For example, in the so-called sensitivity approach [45, 46, 47], is based on the observation that spurious eigenvalues are sensitive to parameter perturbations, while resonances are not. Then, from the modeling of exterior domains, resonances are computed several times with different parameter values  $(a, \sigma_0, \ell)$  and compared. Finally, from the comparison, corresponding eigenvalues are ordered by smallest to largest displacement in the complex plane. It has been observed that this approach is able to identify approximations to true resonances only in small regions of the complex plane. Additionally, the method is expensive as it requires computation of all eigenpairs in a spectral window several times, from where re-meshing and re-assembling of the FE must be performed.

The proposed sorting strategy utilizes Definition 9 for testing each eigenpairs on an already assembled FE mesh. The computation re-uses the pre-computed FE environment, the testing has low memory requirements, and the algorithm is fully parallelizable.

### 7.9. Numerical pseudospectra computation

Computations of the *pseudospectra* provide insight into the behavior of the resolvent of the discretized operator  $F^\gamma$ , allowing us to evaluate its spectral stability. In our computations, we use that  $\sigma_\delta(F^\gamma)$  is the set of all  $z \in \mathbb{C}$  such that

$$s_{\min} F^\gamma(z) < \epsilon, \quad (40)$$

where  $s_{\min} F^\gamma(z)$  denotes the smallest singular value of  $F^\gamma(z)$  [1, Def. 2.10]. For the singular value computations we used SLEPc [43].



$\epsilon_\infty = 1$	$\omega_p = 9.03$	-
$f_0 = 0.76$	$\omega_0 = 0$	$\gamma_0 = 0.053$
$f_1 = 0.024$	$\omega_1 = 0.415$	$\gamma_1 = 0.241$
$f_2 = 0.01$	$\omega_2 = 0.83$	$\gamma_2 = 0.345$
$f_3 = 0.071$	$\omega_3 = 2.969$	$\gamma_3 = 0.87$
$f_4 = 0.601$	$\omega_4 = 4.304$	$\gamma_4 = 2.494$
$f_5 = 4.384$	$\omega_5 = 13.32$	$\gamma_5 = 2.214$

Table 3: Drude Lorentz data for Gold, taken from [48], with time convention  $e^{-i\omega t}$ .

## 8. Applications to metal-dielectric nanostructures

In this section we study four interesting metal-dielectric configurations, from where numerical approximations to resonances and resonant modes are computed. Consecutively, eigenpairs are tested and solutions are sorted according to their corresponding pseudospectrum indicator (39). The sorting strategy is tested on problems where exact pairs are known. Additionally, we consider as reference problem a test case used in [47].

The first three configurations serve as benchmarking strategies for non-dispersive and piecewise constant material properties. Then, we apply the sorting algorithm on a configuration introduced in [41] where a metal coating is motivated from realistic applications in nano-photonics. Here, three different relative permittivity models are used:  $\epsilon_v := 1$  (*Vacuum*),  $\epsilon_s := 2$  (*Silica*), and  $\epsilon_{metal}$  (*Gold*), modeled by a sum of Drude-Lorentz terms (7). For  $\epsilon_{metal}$  we use the data given in table 3 gathered in [48]. This model of Gold has been extensively tested and has validity for  $\omega \in [0.5, 6.5] \text{ eV}$ , where *eV* denotes *electron volt*.

We introduce a demanding configuration where the refractive index is a continuous function of space motivated from the so-called *graded materials*. Finally, we consider an acoustic benchmark problem in  $\mathbb{R}^3$ .

### 8.1. Modeling details

In finite precision arithmetic we prefer to work with dimensionless quantities, where we transform from dimensionless variables to physical variables (denoted with  $\sim$ ). We use common physical constants in SI units:  $\hbar$  is the scaled Planck's constant,  $c$  is the speed of light in vacuum, and  $e$  is the electron charge. In the numerical computations, we use the scaling factors  $W = eV/\hbar$  in *Hertz* and  $L = 2\pi c/W$  in *meters*. Then, we define the dimensionless quantities

$$x = \frac{\tilde{x}}{L}, \quad \omega = \frac{\tilde{\omega}}{W} \quad \text{satisfying} \quad LW = 2\pi c. \quad (41)$$

The resulting length factor is  $L = 1239.842 \text{ nm}$ , from where our spectral window becomes numerically equivalent to *eV* scaling.

### 8.2. Benchmark in 1D: Slab problem

In [3] we introduced a sorting strategy based on Definition 5 but performing computations only inside  $\Omega_r$ . As suggested by (32) and (39), computations can be also performed in  $\Omega_0$ , and it is natural to ask whether or not the sorting scheme performs worse if air is included in the evaluation. Then, we numerically test the solutions to the LS formulation by enlarging the computational

domain to include air. If the LS would exhibit undesired spurious eigenvalues, this would render the method unreliable for detection of spurious pairs.

The following problem has been considered by several authors including [49, 20]. Define for  $n_1 \neq 1$  the piecewise constant function  $n$  as

$$n(x) = \begin{cases} n_1 & \text{if } |x| \leq 1 \\ 1 & \text{if } |x| > 1 \end{cases} \quad (42)$$

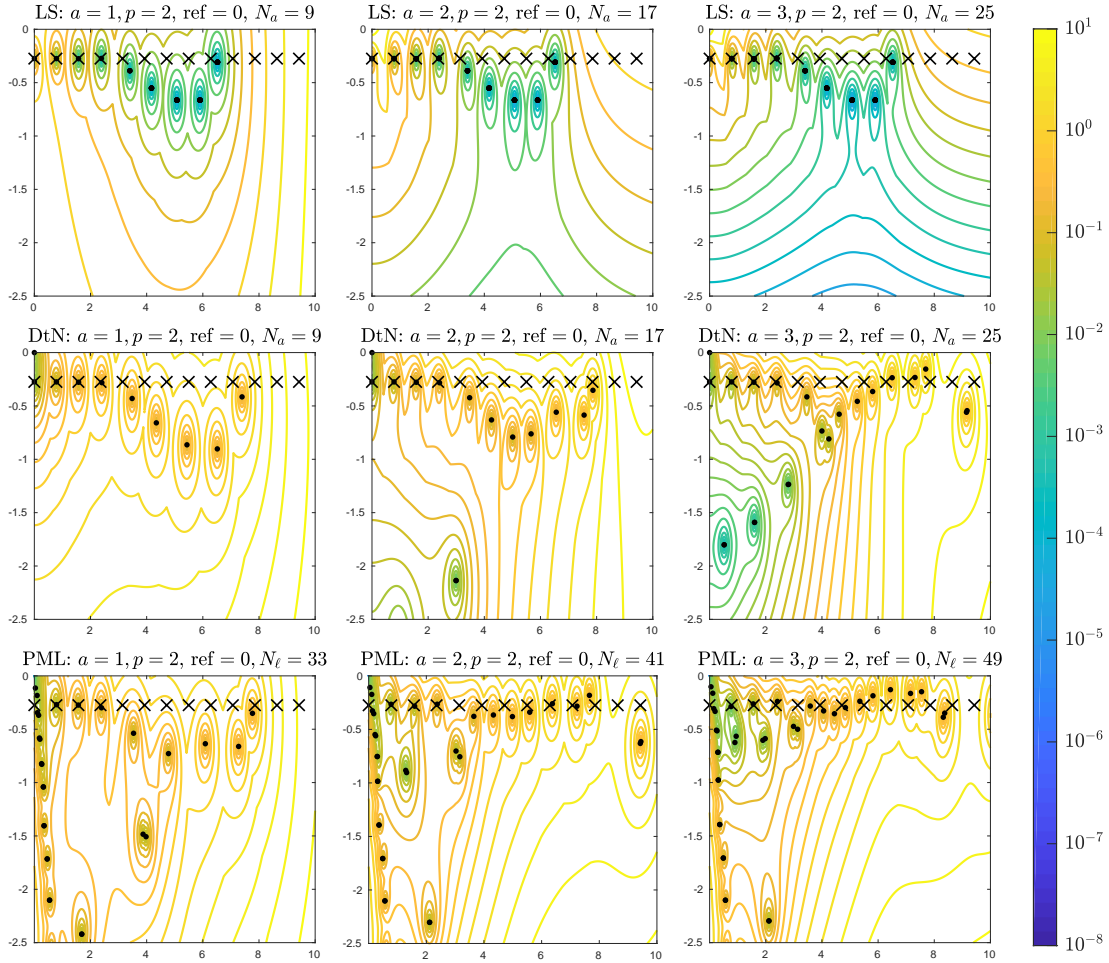


Figure 2: *Pseudospectrum for the TM Slab problem: We illustrate for discretizations with fixed  $p, h, \ell$  the effect of including air regions for the DtN, PML and Lippmann-Schwinger formulations. For reference, we mark with crosses ( $\times$ ) exact eigenvalues.*

The corresponding exact resonances of (12)-(13) for TM polarization are given by

$$e^{4in_1\omega} = \mu^2, \quad \omega_m = \frac{\pi m - i\text{Log}(\mu)}{2n_1}, \quad \mu = \frac{n_1 + 1}{n_1 - 1}, \quad (43)$$

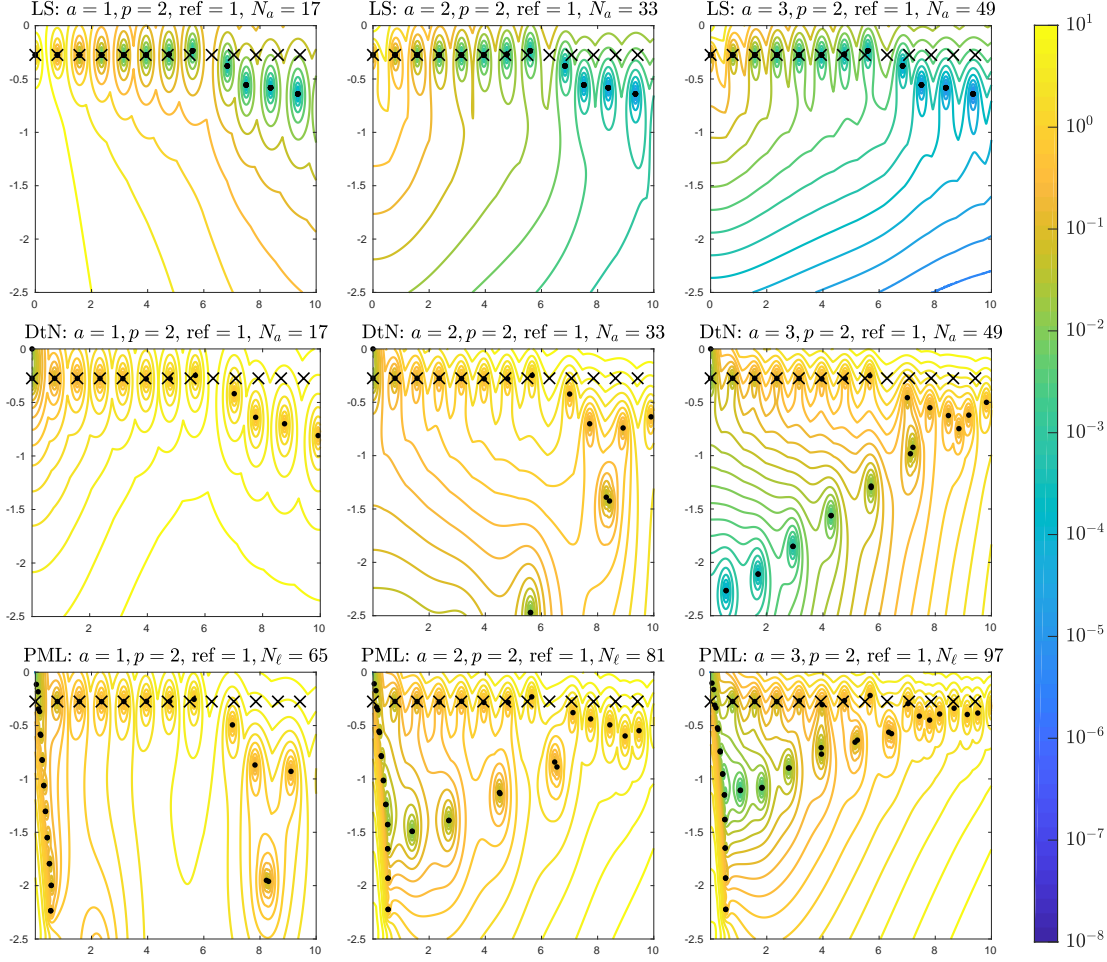


Figure 3: *Pseudospectrum for the TM Slab problem: We illustrate for discretizations with fixed  $p, h, \ell$  the effect of including air regions for the DtN, PML and Lippmann-Schwinger formulations. For reference, we mark with crosses ( $\times$ ) exact eigenvalues.*

*Results:* We start by discussing the stability of the spectrum of the DtN, PML and LS formulations. Namely, the discretization in (26), inherits the property described in Remark 1. Then, it is expected that the spectrum of the LS formulation is not sensitive to perturbations of  $a$  in the sense discussed in Section 2.2.

The number of eigenvalues in a fixed region of the complex plane, and the location of eigenvalues that remain for all perturbations. The proposed experiment is similar to the one presented in [3, Figs 4.1, 5.2, 5.5], but now we allow larger domains  $\Omega_a \supseteq \Omega_r$  in the computation of (26). Then, we compute the eigenvalues and pseudospectrum of FE approximations of the Slab problem described in from Section 8.2 for  $a = 1, 2, 3$ , by using the tools introduced in 7.9. As it can be seen in the figures 2, and 3, the number of eigenvalues in the Lippmann Schwinger formulation remained constant for  $a = 1, 2, 3$ . This means that no spurious eigenvalues are added due to the inclusion of

air. Furthermore, from the plots we see that the computed eigenvalues remain unperturbed when increasing  $a$ , which shows that the eigenvalues are not sensitive to perturbations of the domain.

In the same Figure we see that by increasing  $a$ , there is an increase of the number of computed eigenvalues in a fixed region of the complex plane. Additionally, it can be seen that the location of eigenvalues is slightly modified when perturbing  $a$ . These observations lead us to conclude that eigenvalues from the DtN and PML formulations are very sensitive to perturbations of the domain.

### 8.3. Benchmarks in 2D

The next two problems have radial symmetry centered at the origin, and the solutions expressed in polar coordinates  $(r, \theta)$ , will be written in terms of Bessel and Hankel functions of integer order  $m$ . In this simple case outgoing solutions of (9) satisfy

$$u = H_m^{(1)}(a\omega) \begin{pmatrix} \cos m\theta \\ \sin m\theta \end{pmatrix}, \text{ for } x \in \partial B(0, a), \text{ and } m \in \mathbb{Z}, \quad (44)$$

where  $\text{supp}(n - 1) \subset B(0, a)$ . In subsections 8.3.1 and 8.3.3, we present solutions satisfying (9) and (44) for specific permittivity profiles.

#### 8.3.1. Standard benchmark: Single disk problem (SD)

Denote by  $u = u_1$ ,  $n = n_1$  the restrictions of  $u, n$  to  $\Omega_1 := B(0, R)$ , and set  $n = n_2 = 1$  elsewhere. The corresponding exact eigenfunctions to (9) and (44) read:

$$u_1 = N_m J_m(n_1 \omega r) \begin{pmatrix} \cos m\theta \\ \sin m\theta \end{pmatrix}, \quad u_2 = H_m^{(1)}(\omega r) \begin{pmatrix} \cos m\theta \\ \sin m\theta \end{pmatrix}, \quad N_m := \frac{H_m^{(1)}(\omega R)}{J_m(n_1 \omega R)}. \quad (45)$$

The eigenvalues  $\omega$  corresponding to  $m = 0$  are *simple* and those corresponding to  $m > 0$  are *semi-simple* and have multiplicity  $\alpha = 2$ . The exact eigenvalue relationship for TM and TE can be written as

$$J_m(n_1 \omega R) H_m^{(1)'}(\omega R) - g J_m'(\omega R) H_m^{(1)}(\omega R) = 0, \quad (46)$$

where  $g = n_1$ ,  $g = 1/n_1$  corresponds to the TM polarization and TE polarization, respectively. For numerical computations we use  $R = 1$ , and  $a = 2, 3$ . Additionally, we place the disk center a distance  $s = 0.2$  from the origin such that that many terms are needed in the DtN for approximation of resonances.

*Results:* The application of the sorting scheme (9) to this problem give the results presented in Figure 4. Exact eigenvalues are marked with dots and computed eigenvalues are marked with colored circles, where the color is given by the sorting indicator (39). The upper panels present plots for the TM polarization and in the lower panels results for the TE polarization. The left panels are computed by placing the DtN at  $a = 2$ , while  $a = 3$  in the panels on the right, and both discretizations have the same FE up to  $a = 2$ .

From the figure we observe that increasing  $a$  results in an increase in the number of eigenvalues in the given spectral window, which is expected from the discussion in Sec. 8.2. Moreover, the added eigenvalues from  $a = 3$  pollute larger regions in the spectral window compared to  $a = 2$ . This conclusion can also be obtain by noticing that the minimum in  $\tilde{\delta}$  increases for larger  $a$ , which is related to the fact that exponential growth of eigenfunctions become a challenge for FE discretizations.

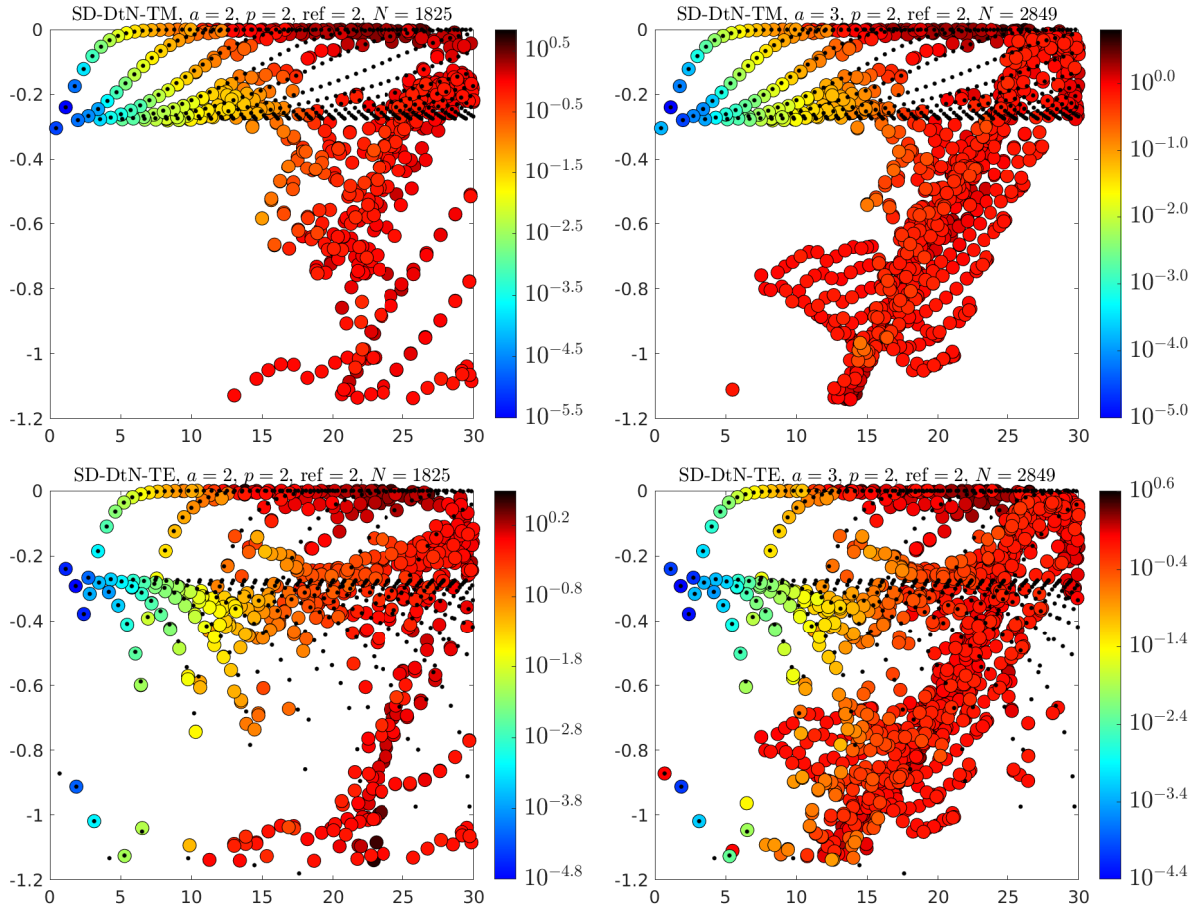


Figure 4: Spectral window showing exact (dots) and FE eigenvalues (circles) the problem described in Section 8.3.1 for TM and TE polarizations. In colors we give  $\tilde{\delta}_m$  corresponding to  $\omega_m^\gamma$  from computations over ten points .

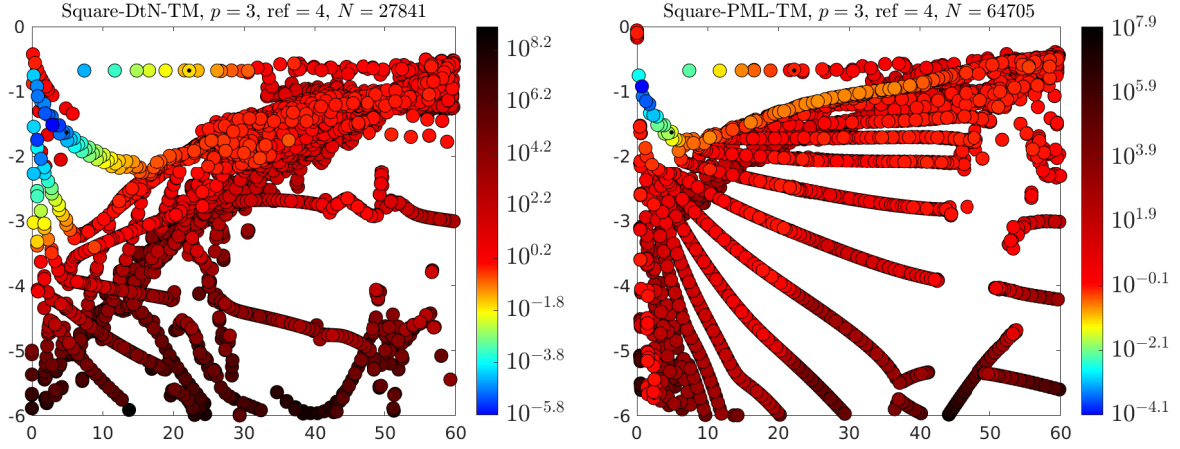


Figure 5: *Spectral window showing two reference eigenvalues (dots) from [47] and FE eigenvalues (circles) of the Single Square problem described in Section 8.3.2 for TM polarization. In colors we give  $\tilde{\delta}_m$  corresponding to  $\omega_m^\gamma$  from computations over ten points.*

Additionally, we see that the values with small indicator values resemble the pattern drawn by the exact eigenvalues. As the value of the indicator increases the corresponding eigenvalues loose this property and become erratic. In this way we can choose a threshold and for example keep eigenvalues  $\omega_m^\gamma$  with  $\tilde{\delta}_m \leq 10^{-2}$  to obtain a set of eigenvalues resembling the behavior of the exact eigenvalues.

Finally, it should be noted that the indicator  $\tilde{\delta}$  can be identified with the FE error in the discretization. Namely,  $\tilde{\delta}_m$  increases with  $\text{Re } \omega_m$ , which is the expected behavior for the FE discretization error of non-dispersive Helmholtz problems [10, 50, 41]. Additionally, eigenvalues with small indicator values appear very close to the exact eigenvalues of the problem.

### 8.3.2. Reference configuration: Single square problem (SS)

For this problem, we set  $\Omega_1 := [-s, s]^2$ ,  $n = n_1$  for  $x \in \Omega_1$  and  $n = 1$  elsewhere. The correct parameters for obtaining the results presented in [47, Fig. 10] are  $s = 1.5$  and  $n_1 = 0.2$  for TM polarization.

*Results:* For this problem, we compute all eigenvalues in the spectral window only once, and cheaply test each computed eigenpair. The results are plotted in Figure 5, by using a DtN in the left panel, and PML in the right panel, where both formulations use the same FE basis in  $\Omega_a$ . Again we can see the effectiveness of using the indicator  $\tilde{\delta}$ . Correct approximations to resonances are easily identified from the overwhelming rest of computed eigenvalues. Additionally, we see that the FE-DtN produces better approximations to resonances than the FE-PML. For example, we mark with dots the two reference values given in [47, Fig. 9], and we see that for the presented discretizations in 5 the DtN marks the reference eigenvalues with lower indicator  $\tilde{\delta}_m$  from (39).

Comparison from the results in Figure 5 against those in [47, Figs. 10, 11, 12] not only illustrates the reliability of the identification of true approximation to resonances by using the scheme in 5, but it also shows its simplicity, flexibility and large coverage in the complex plane.



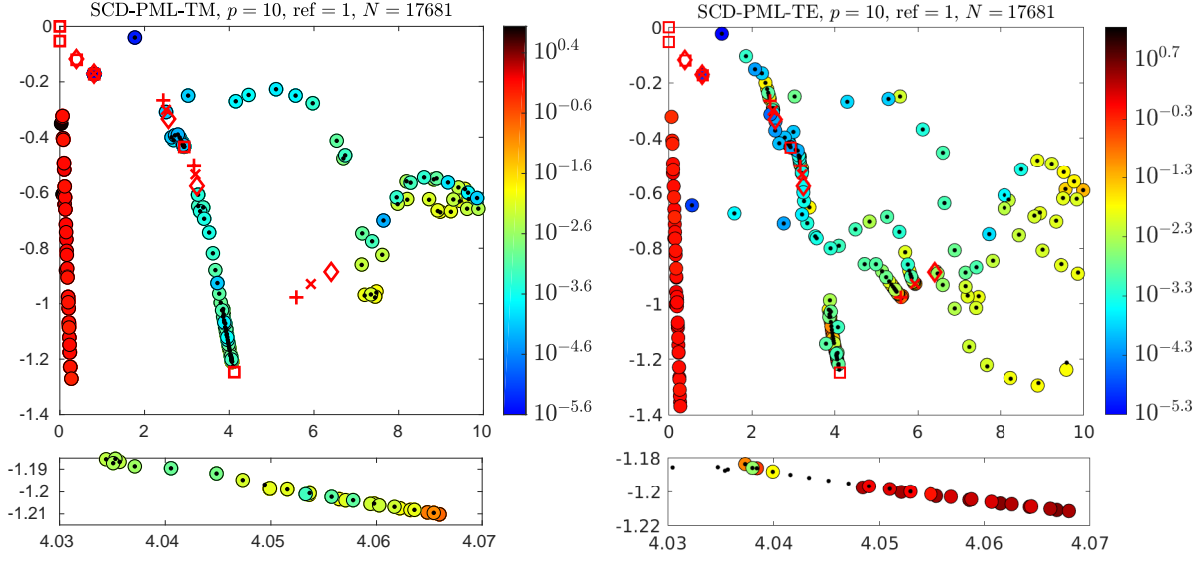


Figure 6: Spectral window showing exact  $\bullet$  and FE eigenvalues  $\circ$  of the Single Coated Disk problem described in Section 8.3.3 for TM and TE polarizations. The poles of  $\epsilon(\omega)$  are given by  $\square$  and its roots  $\epsilon(\omega) = 0$  with  $\diamond$ . Additionally, the plasmonic branch points  $\epsilon(\omega) = -1$  is marked with  $(\times)$ , and  $\epsilon(\omega) = -2$  with  $(+)$ . In colors we give  $\tilde{\delta}_m$  corresponding to  $\omega_m^*$  from computations over ten points.

### 8.3.3. Benchmark with dispersion: Single coated disk problem (SCD)

In this configuration, we consider a resonator consisting of a dielectric disk with a uniform coating layer. The geometry is described by two concentric circumferences of radii  $0 < R_1 < R_2$ , with vacuum as surrounding medium. The inner disk has constant relative permittivity index, and is coated by a layer of gold. We set  $n_1 = \sqrt{\epsilon_s}$ , and  $n_2 := \sqrt{\epsilon_{\text{metal}}}$  is the value such that  $\text{Im}\{n_2\}$  (absorption coefficient) is positive.

The exact solutions satisfy (9) and (44) with  $R \geq R_2$ . The resonance relationship reads

$$\begin{aligned}
 f_1^m(\omega) &= g_1 J_m'(\omega n_1 R_1) H_m^{(1)}(\omega n_2 R_1) - g_2 J_m(\omega n_1 R_1) H_m^{(1)'}(\omega n_2 R_1), \\
 f_2^m(\omega) &= g_3 J_m(\omega n_1 R_1) H_m^{(2)'}(\omega n_2 R_1) - g_4 J_m'(\omega n_1 R_1) H_m^{(2)}(\omega n_2 R_1), \\
 f_3^m(\omega) &= g_5 H_m^{(1)}(\omega n_2 R_2) H_m^{(1)'}(\omega R_2) - g_6 H_m^{(1)'}(\omega n_2 R_2) H_m^{(1)}(\omega R_2), \\
 f_4^m(\omega) &= g_7 H_m^{(1)}(\omega R_2) H_m^{(2)'}(\omega n_2 R_2) - g_8 H_m^{(1)'}(\omega R_2) H_m^{(2)}(\omega n_2 R_2), \\
 F_m(\omega) &:= (f_1^m f_4^m - f_2^m f_3^m)(\omega) = 0,
 \end{aligned} \tag{47}$$

where for TM,  $g := (n_1, n_2, n_2, n_1, 1, n_2, n_2, 1)$ , and for TE,  $g := (n_2, n_1, n_1, n_2, n_2, 1, 1, n_2)$ . The parameters used for the computation are  $R_1 = 0.8$ ,  $R_2 = 1.0$  with scaling factor  $L = 1239.842 \text{ nm}$ .

A complex Newton root finder [51] is then used to compute very accurate approximations of the resonances. For each  $m$  in equation (47), we search numerically the resonances  $\omega_{m,1}, \omega_{m,2}, \dots$  with machine precision stopping criterion. In [41, Table 2], we list a selection of resonances computed from (47).

*Results:* The results for both polarizations are gathered in Figure 47. Here, we observe typical behavior of dispersive resonators *i)* there exist clustering of eigenvalues close to the poles and zeros of the Drude-Lorentz model (7), *ii)* in the TE polarization we have clustering of eigenvalues to the so-called *plasmonic branch points* of the model, which are those values  $\omega$  such that  $\epsilon_{\text{metal}}(\omega) = -\epsilon_j$ ,

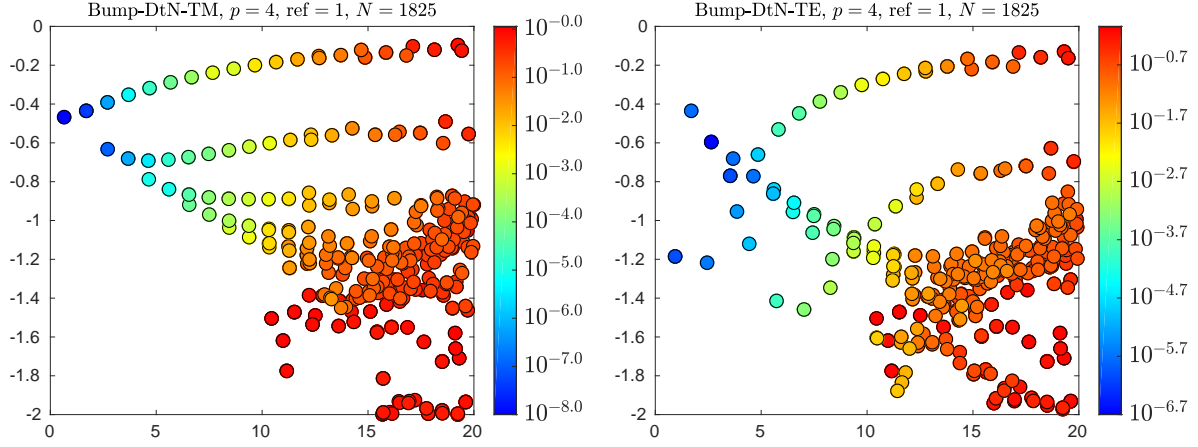


Figure 7: Spectral window showing computed FE eigenvalues (circles) of the Bump problem described in Section 8.3.4 for TM and TE polarizations. In colors we give  $\tilde{\delta}_m$  corresponding to  $\omega_m^\gamma$  from computations over ten points.

with  $j = 0, 1$ . In other words,  $-\epsilon_{\text{metal}}(\omega)$  matches the value of a neighboring dielectric constant (juncture). In the figure, the bottom panels are close up windows showing such accumulations and the corresponding values for the resulting eigenpair indicator  $\tilde{\delta}_m$ . As expected, the value of  $\tilde{\delta}_m$  increases when approaching a critical value (pole, or zero), this behavior is expected since close to a critical point the value  $|n(\omega)\omega|$  increases and the resulting eigenfunction oscillates more rapidly, and the FE error increases. This is further discussed in [41].

#### 8.3.4. Configuration with continuous $n(x)$ : Bump problem

Consider the following refractive index:

$$n(x) = \begin{cases} 1 + P_3(|x|) & 0 \leq |x| \leq R \\ 1 & |x| > R \end{cases} \quad (48)$$

subject to the compatibility conditions:  $P_3(0) = 1$ ,  $P_3(R) = 0$ ,  $P'_3(0) = 0$ ,  $P'_3(R) = 0$ , and  $R = 1$ .

#### 8.4. Acoustic benchmark in 3D: Single ball problem (SB)

This case is analogous to the Single Disk problem 8.3.1 with  $d = 3$ .

Denote by  $u = u_1$ ,  $n = n_1$  the restrictions of  $u, n$  to  $\Omega_1 := B(0, R)$ , and set  $n = n_2 = 1$  elsewhere. The corresponding exact outgoing resonant modes of (9) read:

$$u_{m\ell}(r, \theta, \phi) = \begin{cases} N_m j_m(n_1 \omega r) Y_\ell^m(\theta, \phi), & r \leq R \\ h_m^{(1)}(\omega r) Y_\ell^m(\theta, \phi), & r > a \end{cases}, \quad |\ell| < m, \quad N_m := \frac{h_m^{(1)}(\omega R)}{j_m(n_1 \omega R)}. \quad (49)$$

The eigenvalues  $\omega$  corresponding to  $m = 0$  are *simple* and those corresponding to  $m > 0$  are *semi-simple* and have multiplicity  $\alpha = 2m + 1$ . The exact eigenvalue relationship can be written as

$$j_m(n_1 \omega R) h_m^{(1)'}(\omega R) - n_1 j_m'(\omega R) h_m^{(1)}(\omega R) = 0. \quad (50)$$

*Results for problems 8.3.4, and 8.4:* The results gathered in Figures 7 and 8, confirm the positive results from the application of the sorting scheme 9 pointed out in former discussions of



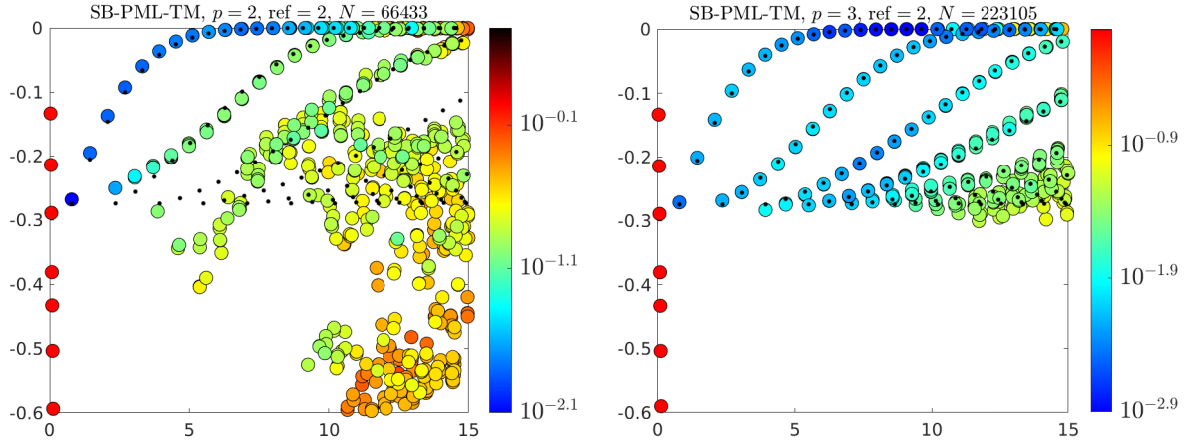


Figure 8: Spectral window showing exact (dots) and FE eigenvalues (circles) the Single Ball problem described in Section 8.4 for TM and TE polarizations. In colors we give  $\tilde{\delta}_m$  corresponding to  $\omega_m^\gamma$  from computations over ten points.

this section. Additionally, we mention that obtaining the results from 8, is a very challenging task. Namely, the FE matrices are denser for  $d = 3$  compared with  $d = 2$ , which results in a high demand of memory per used shift. Additionally, multiplicities can be very large, what translates that in order to compute sufficient number of eigenvalues, one needs to increase the number of Krylov vectors for the computation compared to the two dimensional case. In turn, we end up with a high demand in memory. In our case, it took ARPACK around 28 Gb of ram for each shift consisting of the computation of ten eigenpairs.

The results in the figures illustrate a clear method to sort the computed eigenpairs by using the pseudospectrum indicator (39) effectively, and can then be used to remove pairs with  $\tilde{\delta}_j > \delta_{TOL}$ , with  $\delta_{TOL}$  a chosen threshold.

## 9. Conclusions

We have presented a sorting scheme, based on the Lippmann–Schwinger equation, for the removal of spurious scattering resonant pairs in  $\mathbb{R}^d$  Helmholtz problems. For all computations and for TM and TE polarizations, numerical experiments on a broad range of benchmarks motivated by applications illustrate that the sorting scheme can detect true resonances at low computational cost.

## Acknowledgments

This work is funded by the Swedish Research Council under Grant No. 621-2012-3863.

## References

- [1] Lloyd N. Trefethen and Mark Embree. *Spectra and Pseudospectra: The Behavior of Nonnormal Matrices and Operators*. Princeton University Press, July 2005.
- [2] E. B. Davies. Pseudospectra of differential operators. *J. Oper. Th.*, 43:243–262, 1997.

- [3] J. C. Araujo C. and C. Engström. On spurious solutions in finite element approximations of resonances in open systems. *Computers & Mathematics with Applications*, 74(10):2385 – 2402, 2017.
- [4] M. Cessenat. *Mathematical Methods in Electromagnetism*. Series on Advances in Mathematics for Applied Sciences — Vol. 41. World Scientific Publisher, Singapore, 1996.
- [5] R. B. Melrose. *Geometric scattering theory*. Stanford Lectures. Cambridge University Press, Cambridge, 1995.
- [6] Peter D. Lax and Ralph S. Phillips. *Scattering theory*, volume 26 of *Pure and Applied Mathematics*. Academic Press, Inc., Boston, MA, second edition, 1989. With appendices by Cathleen S. Morawetz and Georg Schmidt.
- [7] J. Gopalakrishnan, S. Moskow, and F. Santosa. Asymptotic and numerical techniques for resonances of thin photonic structures. *SIAM Journal of Applied Mathematics*, 69(1):37–63, 2008.
- [8] Braxton Osting and Michael I. Weinstein. Long-lived scattering resonances and bragg structures. *SIAM Journal of Applied Mathematics*, 73(2):827–852, 2013.
- [9] Chiu-Yen Kao and Fadi Santosa. Maximization of the quality factor of an optical resonator. *Wave Motion*, 45(4):412–427, 2008.
- [10] F. Ihlenburg. *Finite element analysis of acoustic scattering*. Applied mathematical sciences. Springer, New York, 1998.
- [11] X. Wang, Y. Deng, Q. Li, Y. Huang, Z. Gong, K.B. Tom, and J. Yao. Excitation and propagation of surface plasmon polaritons on a non-structured surface with a permittivity gradient. *Light Sci. Appl.*, 5(12), 2016.
- [12] Olaf Steinbach and Gerhard Unger. Combined boundary integral equations for acoustic scattering-resonance problems. *Math. Methods Appl. Sci.*, 40(5):1516–1530, 2017.
- [13] Thorsten Hohage and Lothar Nannen. Hardy space infinite elements for scattering and resonance problems. *SIAM J. Numer. Anal.*, 47(2):972–996, 2009.
- [14] J. C. Araujo C., C. Engström, and E. Jarlebring. Efficient resonance computations for Helmholtz problems based on a Dirichlet-to-Neumann map. *Journal of Computational and Applied Mathematics*, 330:177 – 192, 2018.
- [15] Elias Jarlebring, Karl Meerbergen, and Wim Michiels. Computing a partial schur factorization of nonlinear eigenvalue problems using the infinite arnoldi method. *SIAM Journal on Matrix Analysis and Applications*, 35(2):411–436, 2014. QC 20140908.
- [16] E. Jarlebring, G. Mele, and O. Runborg. The waveguide eigenvalue problem and the tensor infinite Arnoldi method. *ArXiv e-prints*, March 2015.
- [17] E. B. Davies. Non-self-adjoint differential operators. *Bull. London Math. Soc.*, 34(5):513–532, 2002.
- [18] M. Lenoir, M. Vullierme-Ledard, and C. Hazard. Variational formulations for the determination of resonant states in scattering problems. *SIAM J. Math. Anal.*, 23(3):579–608, 1992.
- [19] F. Schenk. *Optimization of Resonances for Multilayer X-ray Resonators*. Göttingen series in x-ray physics. Univ.-Verlag Göttingen, 2011.
- [20] S. Kim and J. E. Pasciak. The computation of resonances in open systems using a perfectly matched layer. *Math. Comp.*, 78(267):1375–1398, 2009.
- [21] Yasuhiko Ikebe. The galerkin method for the numerical solution of fredholm integral equations of the second kind. *SIAM Review*, 14(3):465–491, 1972.
- [22] Junko Asakura, Tetsuya Sakurai, Hiroto Tadano, Tsutomu Ikegami, and Kinji Kimura. A numerical method for nonlinear eigenvalue problems using contour integrals. *JSIAM Lett.*, 1:52–55, 2009.
- [23] W-J. Beyn. An integral method for solving nonlinear eigenvalue problems. *Linear Algebra Appl.*, 436(10):3839–3863, 2012.
- [24] Christian Engström and Luka Grubišić. A subspace iteration algorithm for Fredholm valued functions. *Math. Probl. Eng.*, pages Art. ID 459895, 14, 2015.
- [25] I. Babuška and B. Q. Guo. The h, p and h-p version of the finite element method: Basis theory and applications. *Adv. Eng. Softw.*, 15(3-4):159–174, November 1992.
- [26] C. Schwab. *p- and hp- Finite Element Methods: Theory and Applications in Solid and Fluid Mechanics*. Oxford University Press, 1998.
- [27] Gilbert Strang and George Fix. *An analysis of the finite element method*. Wellesley-Cambridge Press, Wellesley, MA, second edition, 2008.
- [28] P. Solin, K. Segeth, and Ivo D. *Higher-order finite element methods*. Studies in advanced mathematics. Chapman & Hall/CRC, Boca Raton, London, 2004.
- [29] William J. Gordon and Charles A. Hall. Transfinite element methods: Blending-function interpolation over arbitrary curved element domains. *Numerische Mathematik*, 21(2):109–129, Apr 1973.
- [30] William J. Gordon and Charles A. Hall. Construction of curvilinear co-ordinate systems and applications to mesh generation. *International Journal for Numerical Methods in Engineering*, 7(4):461–477, 1973.

- [31] J. T. Oden and J. N. Reddy. *An introduction to the mathematical theory of finite elements*. Wiley-Interscience [John Wiley & Sons], New York-London-Sydney, 1976. Pure and Applied Mathematics.
- [32] Begnaud Francis Hildebrand. *Introduction to Numerical Analysis: 2Nd Edition*. Dover Publications, Inc., New York, NY, USA, 1987.
- [33] P. Solin, K. Segeth, and I. Dolezel. *Higher-order finite element methods*. Studies in advanced mathematics. Chapman & Hall/CRC, Boca Raton, London, 2004.
- [34] G. Alzetta, D. Arndt, W. Bangerth, V. Boddu, B. Brands, D. Davydov, R. Gassmoeller, T. Heister, L. Heltai, K. Kormann, M. Kronbichler, M. Maier, J.-P. Pelteret, B. Turcksin, and D. Wells. The `deal.II` library, version 9.0. *Journal of Numerical Mathematics*, 26(4):173–183, 2018.
- [35] D. Colton and R. Kress. *Integral Equation Methods in Scattering Theory*. John Wiley & Sons, New York, 1983.
- [36] Hideaki Kaneko and Yuesheng Xu. Gauss-type quadratures for weakly singular integrals and their application to Fredholm integral equations of the second kind. *Math. Comp.*, 62(206):739–753, 1994.
- [37] Ran Duan and Vladimir Rokhlin. High-order quadratures for the solution of scattering problems in two dimensions. *Journal of Computational Physics*, 228(6):2152 – 2174, 2009.
- [38] Akash Anand, Ambuj Pandey, B.V. Rathish Kumar, and Jagabandhu Paul. An efficient high-order nyström scheme for acoustic scattering by inhomogeneous penetrable media with discontinuous material interface. *Journal of Computational Physics*, 311:258 – 274, 2016.
- [39] E. Jarlebring, W. Michiels, and K. Meerbergen. A linear eigenvalue algorithm for the nonlinear eigenvalue problem. 122(1):169–195, 2012.
- [40] E. Jarlebring, G. Mele, and O. Runborg. The waveguide eigenvalue problem and the tensor infinite Arnoldi method. Technical report, KTH Royal Institute of Technology, 2015. arxiv preprint.
- [41] Juan C. Araujo C, Carmen Campos, Christian Engström, and Jose E. Roman. Computation of scattering resonances in absorptive and dispersive media with applications to metal-dielectric nano-structures, 2019.
- [42] S. Güttel and F. Tisseur. The nonlinear eigenvalue problem. *Acta Numerica*, 26:1–94, 2017.
- [43] V. Hernandez, J. E. Roman, and V. Vidal. SLEPc: A scalable and flexible toolkit for the solution of eigenvalue problems. *ACM Trans. Math. Software*, 31(3):351–362, 2005.
- [44] S. Balay, W. D. Gropp, L. C. McInnes, and B. F. Smith. Efficient management of parallelism in object oriented numerical software libraries. In E. Arge, A. M. Bruaset, and H. P. Langtangen, editors, *Modern Software Tools in Scientific Computing*, pages 163–202. Birkhäuser Press, 1997.
- [45] B. Kettner and F. Schmidt. The pole condition as transparent boundary condition for resonance problems: detection of spurious modes. In *Physics and Simulation of Optoelectronic Devices XIX*, volume 7933, page 79331B. Proc. SPIE, 2011.
- [46] Benjamin Kettner. *Detection of spurious modes in resonance mode computations*. PhD thesis, 2012.
- [47] Lothar Nannen and Markus Wess. Computing scattering resonances using perfectly matched layers with frequency dependent scaling functions. *BIT Numerical Mathematics*, 58(2):373–395, Jun 2018.
- [48] A. D. Rakić, A. B. Djurišić, J. M. Elazar, and M. L. Majewski. Optical properties of metallic films for vertical-cavity optoelectronic devices. *Appl. Opt.*, 37(22):5271–5283, Aug 1998.
- [49] Braxton Osting and Michael I. Weinstein. Long-lived scattering resonances and Bragg structures. *SIAM J. Appl. Math.*, 73(2):827–852, 2013.
- [50] M. Ainsworth. Discrete dispersion relation for hp-version finite element approximation at high wave number. *SIAM Journal on Numerical Analysis*, 42(2):553–575, 2005.
- [51] A. Ben-Israel L. Yau. The Newton and Halley methods for complex roots. *The American Mathematical Monthly*, 105(9):806–818, 1998.